Computer Aided Design and Fabrication of Magnetic Composite Multilayer Inductors

Robert Stanley Fielder

Thesis submitted to the Faculty of the Virginia Polytechnic Instituted and State University in Partial Fulfillment of the Requirements for the degree of

Masters of Science in
Materials Science and Engineering

Guo-Quan Lu, Chair
Jacobus Daan van Wyk
Jesse J. Brown
Carlos T.A. Suchicital

December 4, 2000
Blacksburg, Virginia

Keywords: Magnetic, Multilayer, Inductor, Ferrite, Computer Modeling

Computer Aided Design and Fabrication of Magnetic Composite Multilayer Inductors

Robert S. Fielder

(Abstract)

Computer modeling using finite element analysis (FEA) was performed to examine the effects of constructing multilayered thick film inductors using an artificially modulated magnetic composite structure. It was found that selectively introducing regions of low permeability material increased both the inductance and the current carrying capacity compared to thick film inductors made with single material magnetic cores. Permeabilities of the composite cores ranged from 1 to 220. The frequency for the models ranged from 0 to 5.0 MHz. Experimental devices were constructed using thick film screen printing techniques and characterized to validate the models and to determine the effectiveness of the design modifications. Quantitative comparisons were made between inductors of single permeability cores with inductors produced with magnetic composite cores. It was found that significant (> 130%) increases could be gained in saturation current with only a 12% decrease in inductance. It was found that the key parameters affecting performance were 1) the placement of low permeability regions, 2) the extent of non-uniform flux distribution within the structure, and 3) the volume fraction of low permeability material.

Dedication

I would like to dedicate this work to my lovely wife, Linda Denise Fielder, who has been my chief advocate and encourager during my educational career, and to my Lord Jesus Christ who died for my sins that I may have eternal life.

Acknowledgments

The author owes the quality of this work to the assistance of many generous people. Dr. Guo-Quan Lu served as the graduate committee chair, and provided continued guidance and mentorship throughout most of the author's undergraduate and graduate career. Dr. Jacobus D. van Wyk and Mr. Johan Strydom provided key insights into the interpretation of the finite element models. Dr. Jesse J. Brown initiated the author's research career by hiring him as an undergraduate research assistant. Dr. Carlos T. A. Suchicital has been another key figure in the author's education, lending technical assistance and expert advice on numerous occasions. Mr. Glenn Skutt at VPT Inc. suggested the design of the apparatus used to measure saturation current. Finally, Mrs. Kelly Stinson-Bagby produced the very descriptive analytical plots. The author would also like to thank the members of the power electronics packaging lab of the Center for Power Electronics Systems at Virginia Tech. They have provided valuable training in the field of electronics packaging, and formed a professional research team of which I was glad to be a part.

This research has spanned most of the author's undergraduate and graduate career and, as such, has received funding from several sources. The Materials Science and Engineering Department at Virginia Tech funded the initial research through the Aspires program, and sponsored a teaching assistanceship. The Bradley Department of Electrical Engineering at Virginia Tech also sponsored a teaching assistanceship and provided lab space and equipment to conduct research. The Center for Power Electronic Systems, a National Science Foundation Engineering Research Center, provided paid undergraduate research experience in addition to providing the electromagnetic modeling software. Finally, Heraeus Cermalloy, Inc. provided the ferrite paste materials used to produce the experimental samples.

Table of Contents

Table of Contents

Table of Contents

List of Figures

List of Figures

List of Tables

I Chapter 1: Introduction

Throughout the history of electronic development, there has been an ever-increasing demand for electronic devices to be more compact and portable, more functional, and more reliable than their predecessors; this demand has been satisfied by two broad methods. First has been the development of electronic materials, such as semiconductors, that have allowed us to advance from vacuum tubes to integrated circuits. Second, there has been much work focused on integrating passive components such as resistors, capacitors, and inductors, to further reduce the size of the overall device[1]. Until recent years, however, little attention has been devoted to the integration of magnetic devices into electronic circuits[2]. The integration of such components has become the next crucial step in reducing the size of electronic devices[3]. One of the most effective methods of integrating magnetic devices into a circuit is through thick film screen-printing[1].

Thick film screen-printing allows the deposition of a material in paste form onto a ceramic substrate. The paste material consists of ceramic or metallic particles suspended in a polymer paste. After printing, the paste undergoes a heat treatment that ultimately burns off the polymer and densifies, or sinters, the ceramic or metallic material through inter-particle diffusion. The result is a dense pattern formed from the ceramic or metallic material. Using this technique, a conducting coil can be printed onto a layer of ferrite (magnetic ceramic), and then covered with another layer of ferrite to form an inductive coil. Successive layers can be printed to increase the inductance of the device.

The thick film process can be easily integrated into a hybrid circuit. After printing the final magnetic layer, the printed magnetic device can be covered with a dielectric layer and a circuit pattern can be printed on top. The magnetic device then becomes part of the substrate structure. Resistors and capacitors can also be printed using this method so that, in principle, all of the circuit's passive devices could be printed into part of the substrate, delivering a level of integration that provides an order of magnitude in size reduction while maintaining a slim profile.

A. Context of research

1.) Applications of magnetic devices

Magnetic devices such as inductors and transformers are found in virtually every electronic device produced. Their applications range from micro-electromechanical systems (MEMS) used for high frequency switching, to large high power inductors used for power conversion. In most of these applications, the size and weight of the entire system is of great importance from both a performance and fuel efficiency point of view. For example, satellites use many magnetic devices to convert power from their solar cell arrays to a high current power supply. It is extremely costly to lift the heavy magnetic cores, usually used in such power applications, into orbit. High performance density is also highly desired from a volumetric point of view. Portable wireless electronic devices such as portable telephones are driving the telecommunications market and the limits of high performance density. As higher levels of functionality are added to these devices, the magnetics must be miniaturized. Other applications include implanted devices such as pace makers. In these applications, magnetic devices must be not only small, but highly reliable as well.

The thick film processing techniques used in this research will not be able to produce devices for all of these applications. With continuing research, however, this technique will find a wider range of applications. Additionally, all of the guiding fundamental principles used in this research may be applied to many different types of processes used for inductor fabrication. Thick film inductors currently find applications imbedded in low temperature co-fired ceramic (LTCC) substrates used in portable wireless devices, hybrid thick film substrates used in satellites, and automotive electronics, shielding in electronic devices[4], and others.

The research presented here may also be directly translated to thin film inductors. Indeed, it will be shown that as the size of the magnetic devices is reduced, consideration of the non-linear material characteristics and magnetic field distributions discussed here becomes even more important. Thin film inductors are increasingly being used in radio frequency integrated circuits (RFICs). Spiral inductors are a basic passive element in a monolithic microwave integrated circuit (MMIC)[5]. In these applications, square spiral inductors integrated into a silicon device, and are used for frequency tuning. Thin film inductors are also used in discrete surface-mount devices. Both thin film inductors

and thin film inductance-capacitance (LC) filters are commercially available as surface mount devices[6] designed for use in mobile communications, satellite TV receivers, global positioning (GPS) receivers, vehicle locator systems, frequency discriminating filters, and network matching.

Larger sized magnetic devices, such as power inductors may also benefit from this research. As the volume of magnetic material in these inductors is reduced, consideration must be given to magnetic saturation. Saturation is the upper limit to the capability of carrying flux by a ferromagnetic material[7], and is driven by the amount of current flowing through the magnetic device. Computer power supplies are one of the most important applications that must make use of high current-carrying capacity in a small volume, with very low losses. The current trend in computer processors is increased clock speed (Currently in the GHz range), reduced voltage (currently 2.0 V), and high power current (100 A)[8]. Much of the work presented here is devoted to maximizing the saturation current for a given limited amount of magnetic material.

2.) Development and future trends

The basic development trend in magnetic devices, as with all electronic systems, is to provide the highest performance possible, in the smallest volume, while consuming a minimum amount of power, and above all, to do all this at a minimum cost to the consumer. Devices are required to operate at ever-increasing frequencies. Current portable wireless devices operate in the GHz range. Integrated inductors are being fabricated on a wider range of substrates including silicon and GaAs, for high frequency applications[5]. Higher efficiencies are being required as portable computing applications such as notebook computers and personal data assistants proliferate to minimize the power demand and increase battery life. Another trend is to maximize the functionality of consumer electronic devices. An increasing number of products seek to integrate multiple tasks, especially internet access, into single systems[9]. Increased functionality in smaller volumes drives down the size of magnetic devices. As the size of magnetic devices decreases, a detailed understanding of the non-linear magnetic properties of materials is required.

3.) Barriers to future development

For RFICs, a significant barrier to further size reduction is the ability to integrate planar inductors into the integrated circuit. To minimize the size of inductors integrated onto semiconductor devices, multilayer processing techniques have been developed to allow the fabrication of capacitors and inductors together[10]. In this process, capacitors are fabricated directly above a thin film inductor integrated onto a GaAs RFIC. The close proximity of these devices, however, leads to electromagnetic interference. To understand and minimize such interference, detailed electromagnetic modeling must be performed. Most modeling techniques for inductors integrated into RFICs are based on numerical techniques, curve fitting, or empirical formulae, and therefore are relatively inaccurate[11]. Accurate computer modeling is required to predict the performance of integrated inductors to minimize design time and thereby reduce cost[12].

As mentioned above, future inductors integrated onto semiconductor materials must operate at extremely low loss values to minimize power consumption. At high frequencies, however, significant eddy currents are produced within the Si or GaAs substrates and reduce the inductor's quality factor, Q[13]. The high resistance of the very thin conductive traces used to fabricate the inductor windings also causes losses. Transmission line resistance is exacerbated by inhomogeneous current distribution within the conductor due to the skin and proximity effects, another topic covered in this research. Such losses are not limited to small "on-chip" inductors, but also apply to high power magnetic devices[14]. A detailed understanding of the mechanisms for current distribution and control of the resulting inhomogeneous magnetic flux distribution within the magnetic core is required to minimize the losses of high performance inductors. Another obstacle in optimizing magnetic devices, especially for high frequency applications, is the frequency dependence of the core material's complex permeability[15]. In general, the permeability of polycrystalline ferrite can be described as the superposition of two different magnetizing mechanisms: spin resonance and domain wall motion[16, 17]. At high frequencies, the effective permeability of ferrites decreases, thereby reducing their performance.

B. Goals of this research

The objective of this research is to develop magnetic devices for electronic systems that have a higher volumetric performance and that integrate easily with state of the art hybrid circuit packages. These objectives were addressed in four broad phases of the project. First, analytical predictions were made based on fundamental principles of electromagnetics to show that the performance of small inductors may be improved by using more than one different type of magnetic material to construct the core. Second, electromagnetic modeling was performed to determine a structure that optimizes performance in the above-mentioned areas. Third, test devices were produced according to selected models using standard thick film screen-printing technology. Finally, magnetic devices were tested to evaluate their electromagnetic performance and to determine if experimental results match the model's predictions. A key contribution of this research is the understanding and control of the inhomogeneous magnetic flux distribution in the core due to uneven current distribution in the conductors, and non-linear magnetic properties of the materials used in the core. The use of more than one type of magnetic material in various regions in the core to control the magnetic flux was of special interest.

1.) Overcoming current obstacles

Much research has been performed to improve and optimize the performance of magnetic devices. These efforts can be broadly divided into three areas of effort: 1) electromagnetic modeling, 2) improving the magnetic core materials, and 3) improving the coil structure. This research attempts to address each of these areas and to make novel contributions to them. Examples of each of these areas will now be discussed.

Electromagnetic modeling usually assumes that an inductor is a linear element consisting of the inductance of the inductor as well as parasitic inductance and capacitance between coils and the substrate[11]. Such models assume no saturation in the magnetic material. If an inductor is produced using an air core, however, such an assumption is valid. The use of ferromagnetic materials, however, provides much improved performance over air core inductors[18]. Other modeling methods utilize the inductor's S-parameter which is related to the coupling between conductors in the spiral coil[19, 20]. Due to the complex geometries of planar coil inductors, field-level modeling is rarely

done[21, 22]. Such modeling is required, however, to accurately predict losses in the substrate. In this research, detailed field-level modeling is performed to predict the electromagnetic performance of the test inductors and, specifically, to aid in understanding the flux distribution within a magnetic core.

Many different magnetic materials have been formulated to improve the performance of magnetic cores. Low temperature ferrite epoxies have been produced and evaluated as core materials for thick film planar inductors[23], as well as for electromagnetic shielding of sensitive components. Ferrite pastes have also been developed for use in thick film screen printing onto alumina substrates[23, 24]. In thick film applications, a ferrite powder is suspended in a polymer binder vehicle and screen-printed onto a ceramic (usually alumina) substrate. Typical ferrite materials include Mn-Zn, Ni-Zn, Ni-Cu-Zn, and Li-Zn ferrites[24]. The printed image can be of arbitrary design, with feature sizes down to approximately 0.2 mm. Successive layers may be printed and fired to construct a complex three-dimensional structure. The screen-printing process is used to create the test devices studied in this research. While work on different magnetic materials is extremely important, most thick film inductor applications use only one type of material in a given core. One goal of this research is to show that it is sometimes beneficial to use more than one different type of material in the same core, especially for small-sized inductors.

Work has also been done to improve the performance of planar square-coil inductors by optimizing the layout of the coil[25]. In these methods, the thickness of the conductive traces in the coil is varied from the inner turns to the outer turns. By varying the conductor width, ohmic losses and eddy current losses can be minimized to improve the inductors quality factor. Another method for improvement related layout is to build the inductor on an insulating layer, rather than directly on Si. In this method, the Si wafer below the inductor is heavily doped with Phosphorus (P+) to form an insulating layer[13]. Thus, substrate losses can be minimized. In this research, attention is given to the coil layout, and how that affects the direction of current flow and, hence, coupling between the conductors. Magnetic coupling between the coils is an important factor in an inductor's performance.

2.) Specific applications of this research

While this research focuses on inductors made with thick film materials on a millimeter size scale, the knowledge obtained may be scaled up or down to include both high power inductors and small inductors integrated onto RFICs. The primary contribution of this research is in the careful consideration of the non-linear properties of ferromagnetic materials. The performance of very small inductors may be improved by the use of such materials, and as high-power magnetic devices utilize less material, the non-linear effects will have to be considered. This research will show that as either the inductor size is decreased, or the current is increased, the non-linear effects of the magnetic material will dominate the design process and must be understood.

II. Chapter 2: Procedure

A. Introduction: Strategic overview and guiding principles

In examining the use of a non-homogeneous, or magnetic composite core structure, three primary tools were used. First, an analytical analysis was performed to establish the basis for interpreting the computer models and experimental results. Second, finite element analysis using computer modeling was performed to simulate the effects of placing materials with various magnetic properties in selected locations within the core. Finally, experimental samples were produced using thick film screen-printing techniques to validate the models.

The primary structure under investigation in this project consists of two flat conductive coils, printed parallel to one another, and electrically connected in series. Electrodes are included for electrical testing. Figure [1] shows each layer of the devices that were modeled, constructed, and tested.

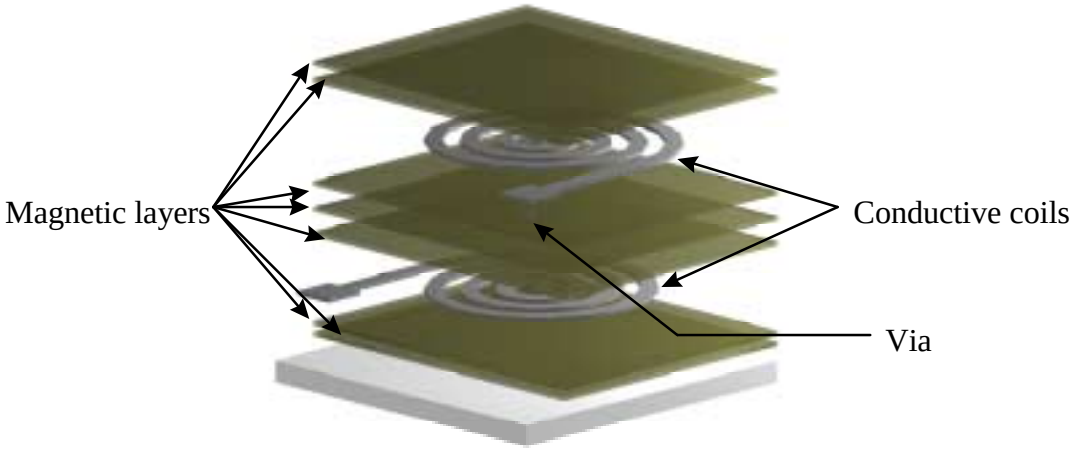

Figure [1]. Target structure, expanded for clarity.

Devices were built on alumina (Al_2O_3) substrates. The first two printed layers were ferrite, to complete the magnetic circuit below the bottom coil. The bottom coil, with its electrode, was printed using a silver conductive paste that was designed to be co-processed with the ferrite. A minimum of three ferrite layers was required to isolate the top and bottom coils. Each ferrite layer was printed with a void, or via, in the center which was filled with a silver paste to provide a path for the

electrical connection between the two coils. The top coil was printed and connected to the second electrode through the via. To complete the magnetic circuit above the top coil, two more ferrite layers were printed.

1.) Addressing specific parameters

The performance of the test inductors under consideration was evaluated using three parameters: 1) inductance, 2) saturation current, and 3) high frequency performance. The basic physics governing these quantities will be introduced now.

a.) Maximizing Inductance

Inductance is proportional to the magnetic permeability of the magnetic material, and the magnetic flux cross sectional area according to the following[26]:

$$L = \frac{d\Phi}{dI} = A\frac{dB}{dI} = \mu \cdot A\frac{dH}{dI} \qquad \text{Eq.[1]}$$

Where:

L = inductance A = area B = magnetic flux density

I = current ϕ = magnetic flux μ = permeability

H = magnetic field strength

Maximizing volumetric inductance, therefore, is accomplished either by increasing the permeability of the magnetic core, or by increasing the area through which the magnetic flux flows.

b.) Maximizing current carrying capacity

The second criterion, maximizing current carrying capacity in a specified volume, is limited by the saturation magnetization of the structure. In a nonlinear ferromagnetic material such as ferrite, after a certain critical magnetic field strength is reached, the material saturates[26]. According to

Ampere's circuital law, the relationship between the magnetic field, H, and the current that sets up the field is given by[26]:

$$I = \oint_{closedpath} \vec{H} \bullet dl \qquad \text{Eq. [2]}$$

Where:

H = magnetic field strength l = magnetic path length I = current

If the magnetic field strength is at saturation for a given current, then the above relationship suggests that increasing the magnetic path length increases the allowed current. After saturation, increasing the field strength results in no increase in the magnetic flux density, and the permeability decreases, which results in decreased inductance. To prevent saturation at high currents, the peak magnetic field must be limited below the saturation level, or the saturation magnetization. To predict if the modeled, magnetic composite, structure saturates at a higher or lower current than a structure with a single magnetic material, the peak flux density is determined. A device with a lower peak flux density saturates at a higher current, thereby increasing the current carrying capacity, or saturation current. Some of the models investigated, which will be discussed shortly, suggested a method to limit saturation in regions of high magnetic field.

c.) Optimizing high frequency operation

The third criterion to consider is operation at high frequencies. At higher frequencies, the conduction of electricity through the silver transmission lines gives an uneven current distribution due to the skin effect and proximity effect. The skin depth of the conductor determines the depth of penetration of the current into the conductor as a function of frequency and is given by the following[26]:

$$\delta = \frac{c}{k\omega} \qquad \text{Eq. [3]}$$

Where:

δ = skin depth c = speed of light in vacuum

ω = frequency k = optical material constant

As the frequency increases, the skin depth decreases; therefore, more of the current is carried along the surface of the transmission lines. The result, in the flat geometry of printed transmission lines, is that current density is highest along the edges which confines the magnetic field to the magnetic material in the vicinity of the transmission line edges, thereby utilizing only the material in those regions for energy storage, and reducing inductance. To increase performance at higher frequencies, structures were designed to more evenly distribute the magnetic field and thereby maximize the use of all available magnetic material.

The proximity effect is the uneven current distribution in a conductor at high frequencies that is in close proximity to other high-frequency conductors. This produces both eddy current losses, and inhomogeneous flux distribution and will be discussed later.

2.) Analytical prediction

The analytical predictions were conducted using fundamental principles of electromagnetics and measured properties of the materials that would be used to produce the test samples. The goal of this analysis was to dispense with the simplifying assumption that magnetic materials behave linearly, and to express the permeability material as a function of both the current contained within a magnetic loop, and the position of the material in the magnetic device.

3.) Finite element modeling

Electromagnetic modeling was performed using Maxwell Field simulator ™, version 7.0.1, from Ansoft, Inc. Advanced models were constructed using a 5-turn coil model, with two magnetic layers

below the bottom coil, two magnetic layers above the top coil, one layer in each coil plane, and three layers between the planes. Two conductive coil planes were stacked in parallel, as in Figure [1]. The model was drawn in two dimensions; the software, then, integrated the two dimensional cross-section around the z-axis to calculate the total inductance. The thickness of the magnetic and conductive layers was set at 10μm, which is approximately the reported fired thickness for these materials. To establish a baseline for comparison, a model was constructed using a single magnetic material with a permeability of $\mu = 220$, which is the highest permeability paste available at this time.

The magnetic permeability of the materials was then varied through the layers. The first series of models examined the effects of allowing the permeability of the material immediately surrounding the transmission lines (above and below the transmission line planes, denoted hereafter as the "cladding layers") to range from 1.0 to 220. A second series varied the permeability of material in the plane of the conducting coils over the same range. Other strategies have been briefly examined, but the above-mentioned structures are of primary interest.

Material parameters of ferrite pastes available from Heraeus Cermalloy were used. This material system was chosen for its wide range of magnetic properties and its cofirability. The conductive traces (transmission lines) were modeled using a pure silver paste designed for use in a multilayer magnetic structure. The current for the models was set at +/- 1.0 A and 2.0 MHz and was based on an estimate of the transmission line's current carrying capacity. The frequency was selected to match a similar application under intensive study at the Center for Power Electronics Systems (CPES) at Virginia Tech. A frequency of 2.0 MHz was also sufficient to demonstrate the skin effect and proximity effect in the transmission lines.

4.) Experimental verification

Experimental inductors were constructed using standard thick film screen-printing techniques. Ferrite pastes as well as silver pastes from Heraeus Cermalloy were used. The paste system used was a low temperature cofired ceramic system. During processing, each printed layer was dried individually at 110 ^{o}C, and fired at 850 ^{o}C. Inductance measurements were made using an impedance analyzer.

B. Analytical prediction

1.) Target structure

For the analytical predictions, the simple geometry of a long, cylindrical conductor was used. This convention simplified the equations, and facilitated a clearer understanding of the physics without complicating the geometry.

2.) Derivation of analytical solution

The following derivation begins with the basic definition for self-inductance, which is our primary parameter of interest, and reduces it to a dependence on the properties of the core material. These properties are then described in terms of the operating conditions and geometry of the magnetic device. It will become clear that the optimum selection and placement of a core material will depend greatly on the geometry and operating parameters of the inductor, and that the performance of many high-density devices may be optimized only through the use of a magnetic composite structure.

First, consider the basic definition of self inductance:

$$L = \frac{d\Phi}{dI} \qquad \text{Eq.[4]}$$

Where:

L = self inductance Φ = total magnetic flux I = current

From this definition, we see that self-inductance is the change in magnetic flux produced for a given change in electric current.

The simple geometry of a long conducting wire will be used to derive the relationship between inductance, and the magnetic properties of the materials surrounding the conductor. For a long conducting wire:

$$\Phi = \oint \vec{B} \cdot \vec{n} da \qquad \text{Eq.[5]}$$

Where:

B = magnetic flux density **n** = unit vector

a = distance from the wire

The magnetic flux density for a given location near the wire is given by:

$$\vec{B} = \frac{\mu_0 I}{2\pi a} \vec{k} \qquad \text{Eq.[6]}$$

Where:

μ_o = permeability of free space I = current **k** = unit vector

Taking the magnitude only:

$$B = \frac{\mu_0 I}{2\pi a} \qquad \text{Eq.[7]}$$

The current carried in the conductor is related to the magnetic field intensity for a given distance away from the wire, and is given by:

$$I = \oint Hdl \qquad \text{Eq.[2]}$$

Where:

I = current contained within the magnetic loop H = magnetic field intensity

l = length of magnetic loop, or magnetic path length

Therefore, for a circular magnetic loop about a long conducting wire:

$$H = \frac{I}{l} = \frac{I}{2\pi a} \qquad \text{Eq.[8]}$$

Substituting Eq[7] into Eq[5], we get:

$$\Phi = \frac{\mu_0 I}{2\pi} \ln(a) \qquad \text{Eq.[9]}$$

Where Φ is the total flux contained within the surface. The above relationships assume that the conductor is contained in a vacuum. We would like to find the incremental contribution of a given section of material, da, at a distance (a) away from the conductor. To do this, we must identify the permeability of the material. The reported permeability of commercially available ferrites is given by the maximum linear permeability. That is the slope of the vector from the origin to the beginning of saturation on the BH curve. We will be utilizing the incremental permeability, which avoids the simplifying assumption that the magnetic material will behave the same at all levels of magnetic field. Graphically, The incremental permeability is the slope of the tangent to the BH curve for a given H field. It varies throughout the entire range of possible magnetic field intensities. See Figure [2] for graphical representation.

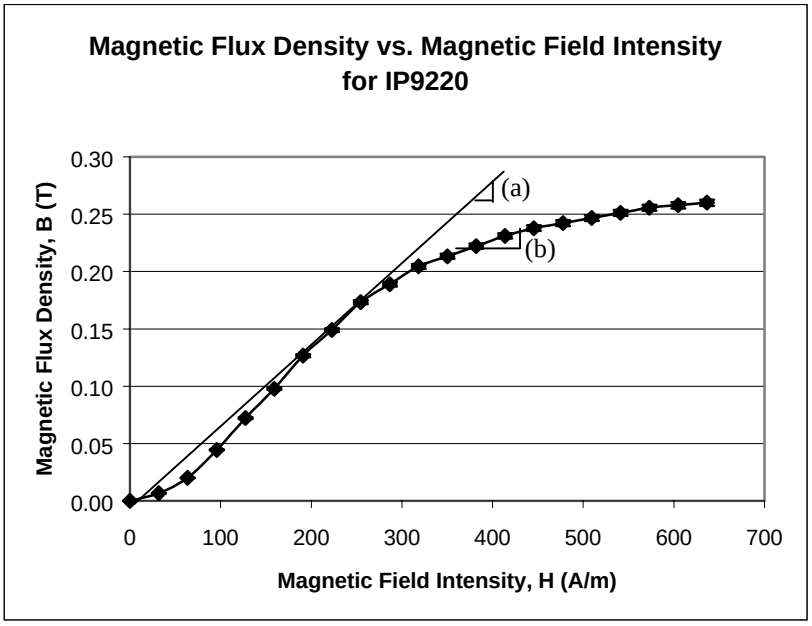

Figure [2] Incremental permeability vs. linear permeability (BH curve). The slope at (a) indicates the linear permeability reported for the material. The slope at (b) indicates the incremental permeability which varies with the applied magnetic field.

Mathematically, the incremental permeability of a non-linear material is defined as the change in magnetic flux density for a given change in magnetic field intensity:

$$\mu = \frac{dB}{dH} \qquad \text{Eq.[10]}$$

The total magnetic flux for a current carrying conductor inside a ferromagnetic material then, can be given by:

$$\Phi = \frac{\left(\frac{dB}{dH}\right)I}{2\pi}\ln(a) \qquad \text{Eq.[11]}$$

From this relationship, we see that the inductance is a function of the incremental permeability of a material at a given location, or distance away from the conductor. We also know that the

incremental permeability is dependant on the magnetic field intensity, H which is given by Eq[8]. Since the incremental permeability, μ, is dependent on H, and H is dependent on magnetic path length, which is a function of distance away from the conductor, then the incremental permeability of a material changes with its location in the magnetic core.

Take, for example, the case of a cylindrical current-carrying conductor (i.e. a wire). The magnetic path length around the wire is given by:

$$l = 2\pi r \qquad \text{Eq.[12]}$$

Where r is the radius of the path. The value of H for a given current varies with r as:

$$H = \frac{I}{2\pi r} \qquad \text{Eq.[13]}$$

Graphically, the magnetic intensity is represented in Figure [3]. The size and current scale for this calculation is based on commercially available chip inductors.

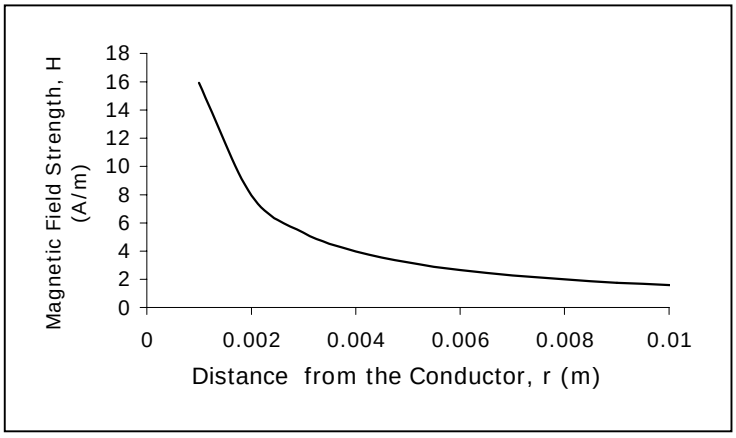

Figure [3] Magnetic field intensity, H, as a function of distance from a cylindrical conductor. Applied current is 100mA.

Since

$$\mu = \frac{dB}{dH} \qquad \text{Eq.[10]}$$

we obtain the graphical representation for μ by taking the first derivative of the experimentally obtained BH curve. Figure[4], shows how permeability varies with H.

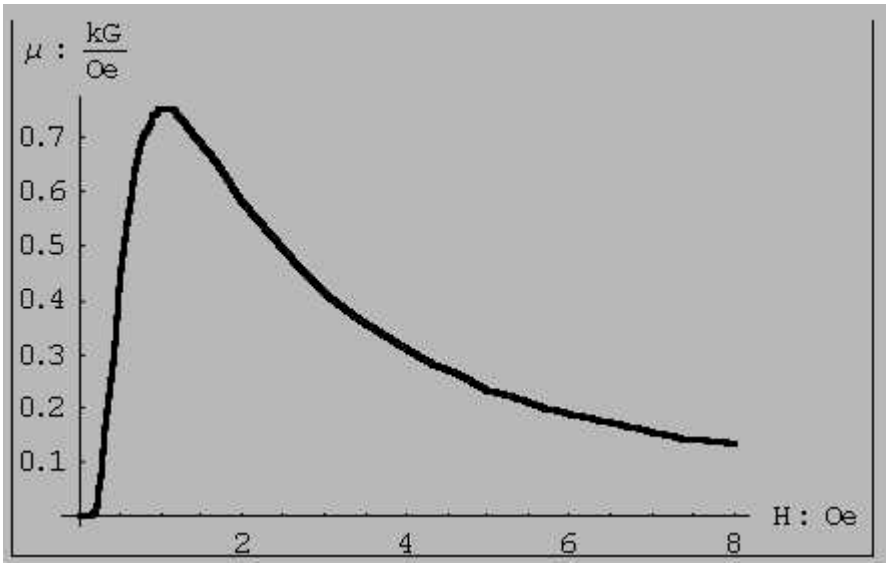

Figure [4] Permeability of IP9220 as a function of applied magnetic field intensity.

The above figure illustrates that a magnetic core material will perform at peak efficiency only if operated at its optimum magnetic field intensity. From the equations cited above, we see that the magnetic field intensity is dependent on the material's position in the core. It can, therefore, be stated, that the magnetic properties of a given material are dependent on its location within the core.

Extending the above hypothesis, it can be shown that different magnetic materials will exhibit optimum magnetic properties at different locations in the core. In other words, for a given location in the core, one material will be operating closest to its optimum value, of permeability, while other

materials will be either saturated, or under magnetized. It follows, then, that the performance of a given magnetic device, such as an inductor, can be optimized only through the use of more than one different type of magnetic material in the core.

Figure[5] shows a family of BH curves experimentally obtained from the materials used to produce experimental samples.

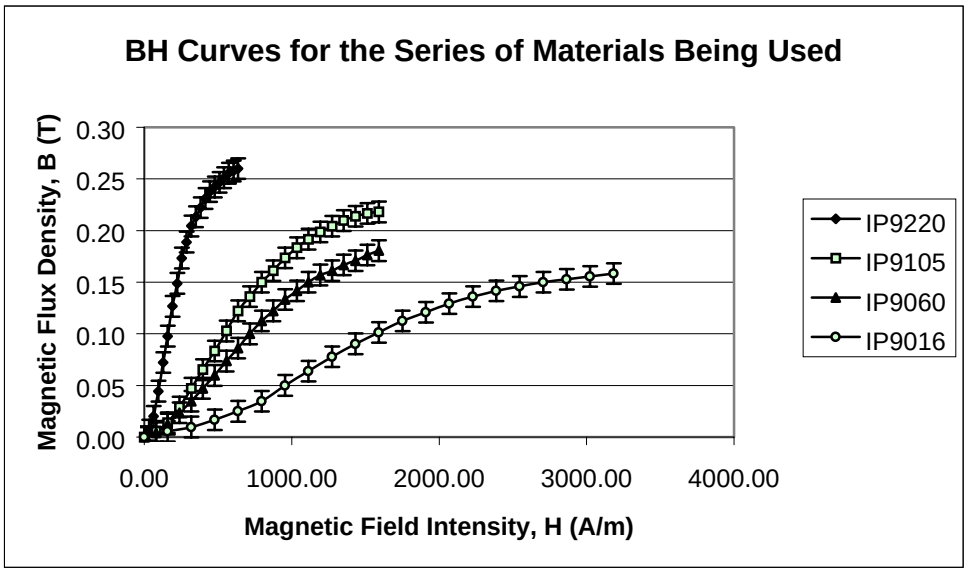

Figure [5] Family of BH curves for the ferrite materials under investigation.

Taking the first derivative of these curves gives permeability as a function of magnetic field intensity, and, by extension, as a function of distance away from the conductor. This is shown graphically in Figure[6a] and Figure [6b].

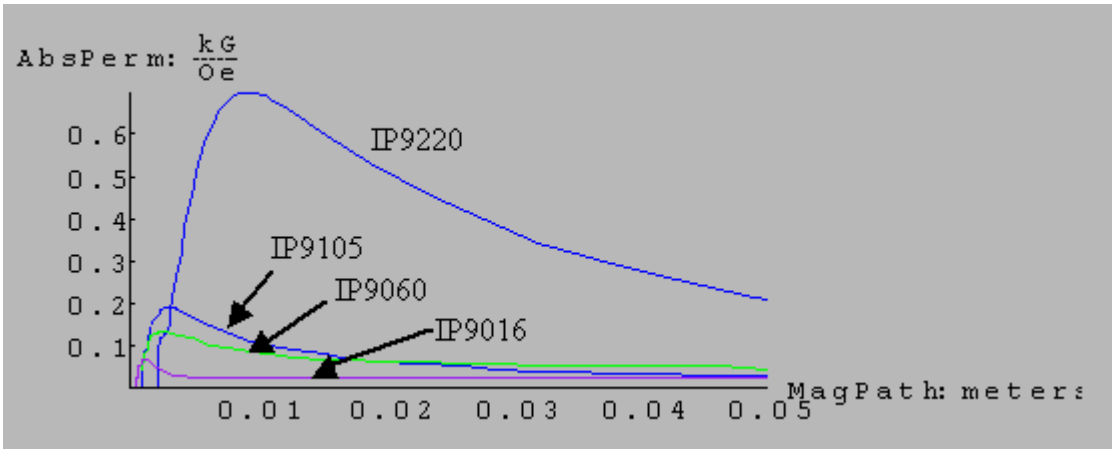

(a)

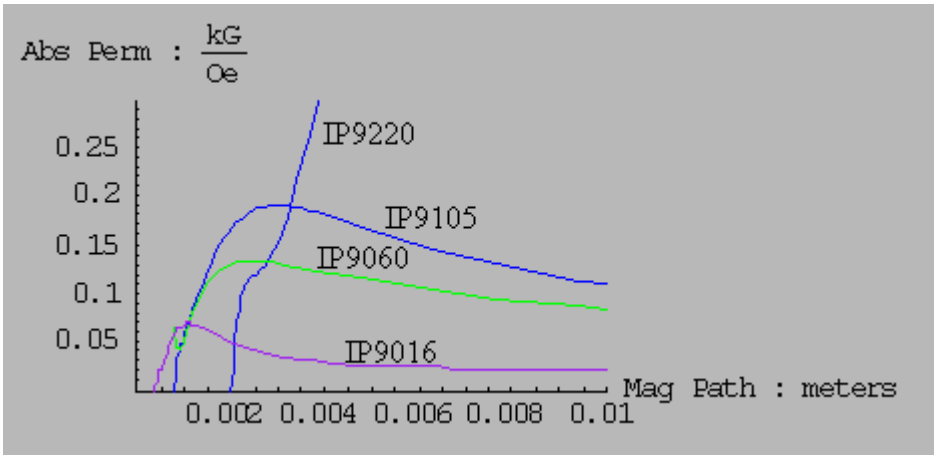

(b)

Figure [6a, and 6b]. Permeablity vs. magnetic path length for the ferrite materials under investigation. Part (a) shows a wide range of path lengths, while part (b) highlights shorter path lengths.

3.) Summary

It has been shown that the magnetic properties of the core material depend on their placement within the core. Optimizing the design of an inductor, therefore, requires the use of more than one different type of material to be used in the core. From measured data of materials to be used in magnetic devices, it will become possible to establish design rules to guide the design of magnetic devices with composite core structures.

C. Finite element modeling

Electromagnetic models were created in two dimensions, representing a cross-section of the inductor to be modeled. The software then "rotated" the cross-section around the vertical (z) axis to produce a three-dimensional structure. Early attempts at producing a detailed three-dimensional model exceeded the computer's ability to solve the model in a reasonable amount of time.

Three basic styles of models were used: 1) simplified cross-sections that modeled only 4 conductive coils, 2) full cross-sections that modeled the same number of coils, nine, that would be used in the experimental samples, and 3) magnetostatic models that combined non-linear magnetic material parameters with an artificial current distribution. The simplified cross-section models were the first used. The purpose of these models was to visualize the flux distribution within the core. The goal of the full cross-section models was to determine if a computer model could predict accurate values of measured inductance if given enough accurate information about the structure.

The composite magnetostatic models were constructed to answer the deficiencies of the software that did not allow the combination of a time-dependent current signal with non-linear material properties. To construct these models, the current distribution across a conductor was determined using one of the previous models. The software allows the analysis of a specified parameter, current density in this case, along a user-defined line. For this analysis, a line was constructed through the center of the conductor. Values for current density were taken from the resulting plot. The conductors in the magnetostatic models actually consisted of 25 separate elements. Each element was assigned a specific current density according to that measured from the eddy current model. The magnetic materials comprising the core were then assigned non-linear characteristics based on hysterisis graph measurements. The resulting "composite" model allowed the combination of non-linear material characteristics with the current distribution found in a device with a time-dependent signal. The primary shortcoming of this model is that neither current nor frequency values may be easily changed.

1.) Modeling setup

Figure [7] shows a cross section of one transmission line each from the top and bottom coils surrounded by layers of magnetic material. This model contained only one type of magnetic material, IP9220[a] ($\mu = 220$). As frequency was increased to 2.0 MHz, it was observed that the electric current distribution through the transmission lines was non uniform, due to the skin effect and proximity effect, with the highest current density existing along the edges of the conductive material. The current concentration along the edges then confined the magnetic field to those regions, leaving the vast bulk of magnetic material devoid of magnetic flux resulting in a poor utilization of the material, since energy was stored only in a small fraction of the volume.

(a)

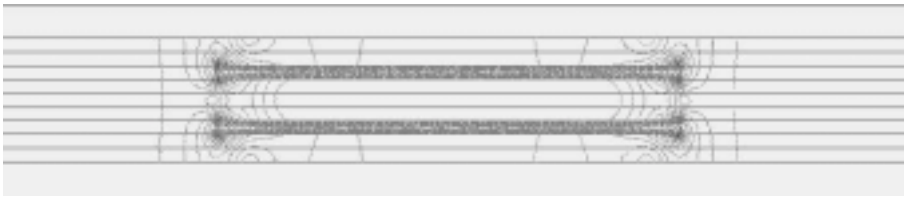

(b)

Figure [7] Cross section of internal coil structure showing single material core with $\mu = 220$, frequency is 2.0 MHz. Part (a) shows the shaded magnetic flux gradient, while part (b) shows the gradient lines.

Figures [8] and [9] show the same cross section but with modified magnetic layers. In Figure [8], low permeability material surrounds the conductive traces, which forces the magnetic flux to flow around the outer magnetic layers. In a right-right structure, this substitution method forced the magnetic flux through the high permeability channel between the conductors, thus utilizing that region. In Figure [9], the low permeability material was substituted into the plane of the conducting coil which had the effect of introducing a distributed air gap in the path of the magnetic flux; The

[a] All ferrite pastes were donated by Heraeus Cermalloy, Inc.

low permeability plane acted as a resistive material to magnetic flux, therefore, a wider cross sectional area was required to pass the same amount of flux.

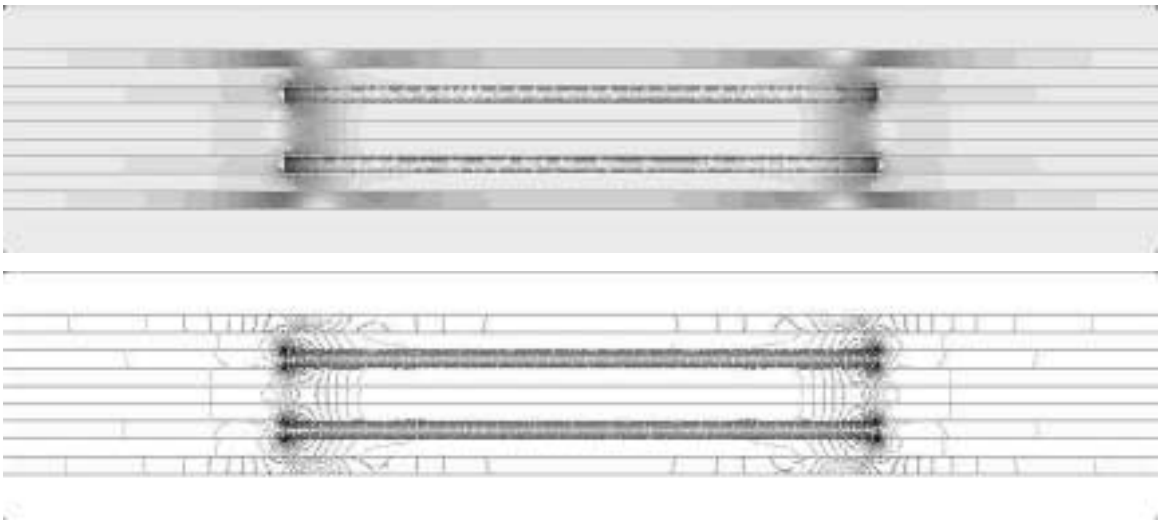

Figure [8] Low permeability magnetic material surrounding coils.

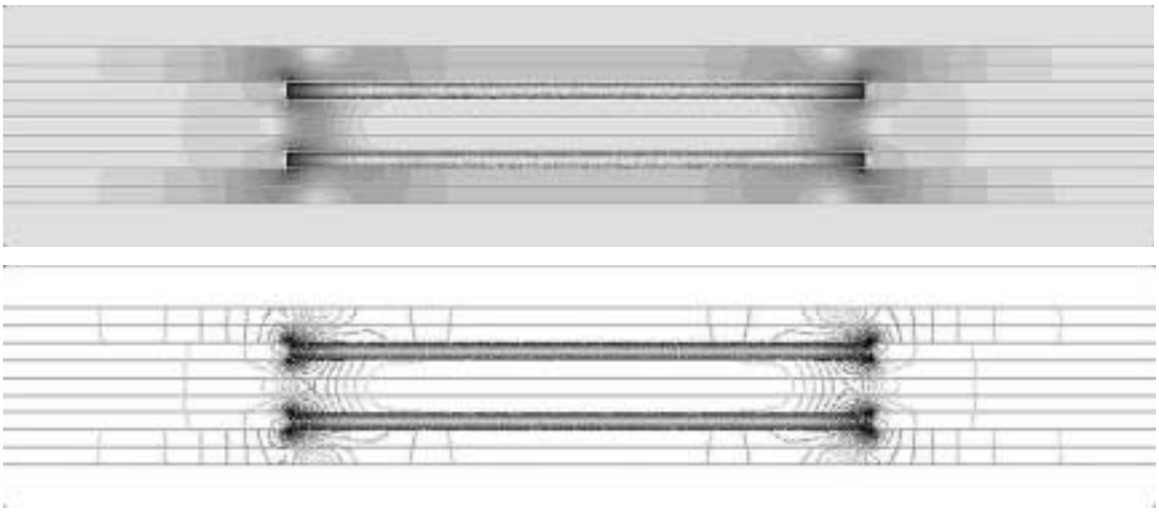

Figure [9] Low permeability material substituted into the transmission line planes.

The first magnetic composite structure, Figure [8], was designed to increase inductance by increasing the utilization of the magnetic material between the conductive traces of parallel planes. The second composite structure, Figure [9], maximized the use of material between conductive traces in the same plane.

a.) Initial modeling

Early models simulated a two dimensional cross section of the parallel coil structure. The material properties used were assumed to be linear, as non-linear data were not available. Figure[10] shows one such model.

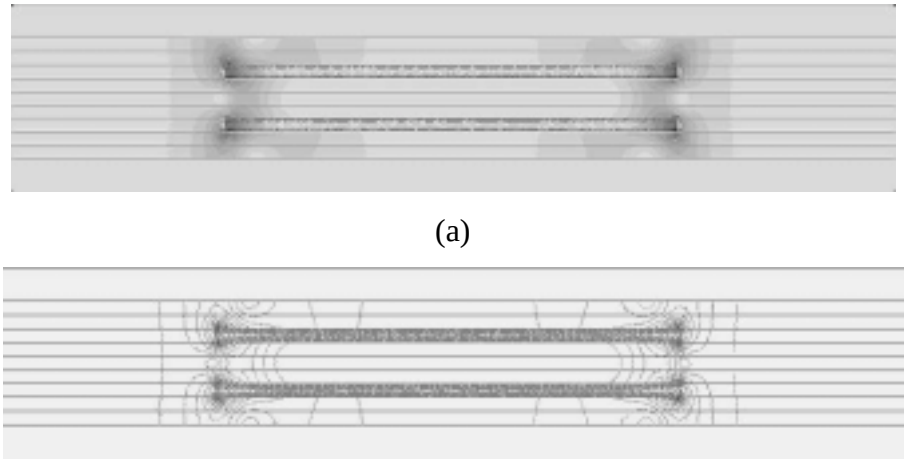

(a)

(b)

Figure [10] Two-dimensional cross-section model showing flux distribution for a core with a single magnetic material with a permeability of $\mu = 220$.

The first series of models were composed of single material cores, having a permeability of 220. The initial parameter of interest was frequency. A series of models was run that varied frequency from zero to 2.0 MHz. The final frequency corresponded to a project for which the thick film inductors were a candidate. Increasing frequency resulted in an inhomogeneous flux distribution in the core, the observation of which will be discussed later.

The next series of models was used to examine the effects on flux distribution when more than one different type of magnetic material was used. The "matrix" material, or the material that composed the bulk of the core, was IP9220 and had a reported permeability of approximately 220. A second material was substituted into one or more layers in the structure. The substitutional layers are denoted hereafter as the cladding layer (CL), separating layer (Sep), and the transmission line layer (TL). See Figures[11] (a), (b), and (c) for a graphical representation of the substitutional

arrangements. For all of the following schematics, dark shaded rectangles represent the conductor cross-sections, lightly shaded rectangles indicate regions of low permeability material, and white rectangles represent layers of high permeability ($\mu = 220$) material.

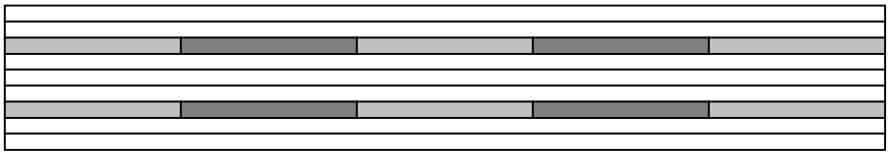

[a]

[b]

[c]

Figure [11] Substitution of low permeability material into different planes. [a] Substitution into the transmission line plane, [b] Substitution into the cladding layers, and [c] Substitution into the separating plane.

Other methods of substitution were considered as well. However, the above-mentioned substitutional methods were the best suited for thick film processing.

b.) 3D structures

The two dimensional structures were adequate to give an approximation of the flux distribution and electromagnetic performance for a simplified structure, however, it was desired to produce a more detailed three dimensional model that would incorporate the exact geometry of the test samples. It was expected that by accurately modeling the actual geometry of the sample parts, a very

accurate prediction of performance could be obtained. To accomplish this goal, a completely detailed three-dimensional model was created to simulate the parallel coil structure. This model proved to be too complex for the computer to solve in a reasonable amount of time and was, therefore, abandoned[b].

c.) 2D structures

The structure of two-dimensional models has evolved from simple 4-turn coils to more advanced composite models consisting of 25 conductive elements per conductor. To further increase accuracy, the modeled dimensions were as close as possible to those measured for the experimental inductors.

d.) Non-linear input

All of the above-mentioned models lacked the non-linear characteristics of the ferrite material and their accuracy, therefore, was limited. The non-linear characteristics (BH curves) of the ferrite material were not available from the manufacturer. The manufacturer did, however, provide bulk samples of material that had been pressed into toroids for other measurements. These samples were then characterized using a hysterisis graph to obtain their BH (magnetic flux density vs. magnetic field strength) curves. The process of obtaining these curves is detailed later. The non-linear data was included in the model in the form of user-defined materials. Maxwell™ allows the use of user-defined materials. The modeling software, however, does not allow the combination of non-linear material properties with a time-dependent (eddy current) signal. Modeling was, therefore, limited to either using non-linear material properties with a DC (magnetostatic) signal, or linear properties using eddy current analysis. The real limit here was that the eddy current analysis was required to approximate the current distribution inside the conductors, and the non-linear material properties were required to predict magnetic saturation, and the resulting redistribution of flux. Further improvement of the model required that these deficiencies be overcome.

[a]For a full, three-dimensional model, a single iteration took over two weeks to complete.

e.) Composite models

One method attempted to address this problem was to create a magnetostatic model wherein the conductors were manually divided into several elements and individually assigned a current density. Using the magnetostatic model allowed the use of non-linear material properties. Dividing the conductors into elements allowed the simulation of the current distribution found in eddy current models. To create this "composite" model, the current distribution of an eddy current model was measured as a profile across the conductors. Each conductor was divided into 25 elements, and the current density in the eddy current model was measured corresponding to each element. In the composite model, these individual current densities were assigned to the 25 elements that made up the conductors. The result was a model that included non-linear material properties, and approximated the current distribution produced by a high frequency current.

The modeling process can be continued to be refined, as several deficiencies still exist, such as the resolution of current distribution, and the managing of the data output.

2.) Summary

In summary, the electromagnetic modeling has evolved from simple two-dimensional models that observed the effects of an electrostatic (DC) current signal, to more complex two-dimensional models that combined both non-homogeneous current distribution in the conductors and non-linear material properties of the magnetic ceramic. Three-dimensional models were attempted and abandoned due to the limitations of the computer hardware.

D. Experimental verification

1.) Structures under investigation

Three primary structures were investigated using experimental samples: 1) parallel "square wave" coil, 2) parallel spiral coil, and 3) single plane spiral coil. These three structures are illustrated in Figures[12] and [13]. Each of these structures was used to examine different effects of using a composite core structure.

Figure [11] Photograph of "square-wave" coil pattern printed on alumina substrate.

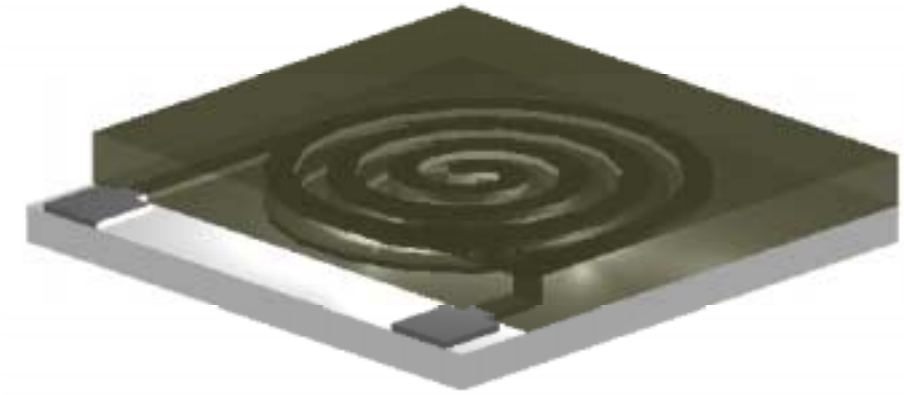

Figure [12]. Cad rendition of a parallel circular spiral inductor. For "Right handed-Right handed" structures, both of the coils spiraled in the same direction. For "Right handed-Left handed" structures, the coils spiraled in opposite directions.

For the parallel square wave coil, a cross section of the conductors, Figure[14c], shows current flowing in the opposite direction of its nearest neighbor conductor. In the parallel spiral coil, the current in a conductive trace is flowing in the same direction as other conductors in the same plane, however, the current in the parallel plane will flow in the same or opposite direction depending on the direction the coil spirals. Two right handed coils have current flowing in opposite directions from one plane to the other, Figure [14a], while a right handed then left handed coil have current flowing in the same direction, Figure [14b]. In the figures that follow, the direction of the circulating magnetic field about a current-carrying conductor is shown. For a clockwise-rotating magnetic field, the current is flowing into the plane of the page. For counter-clockwise magnetic fields, the current is flowing out of the page.

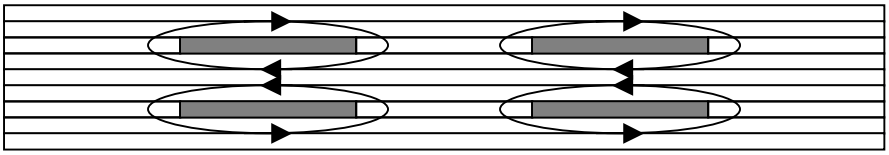

Figure [13a] Magnetic fields in a RR spiral structure.

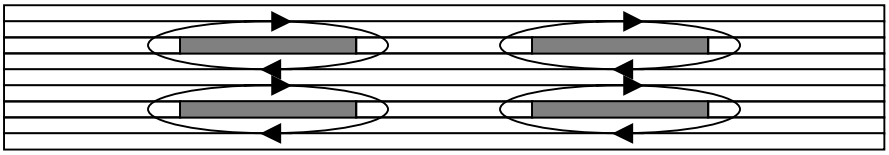

Figure [14b] Magnetic fields in a RL spiral structure.

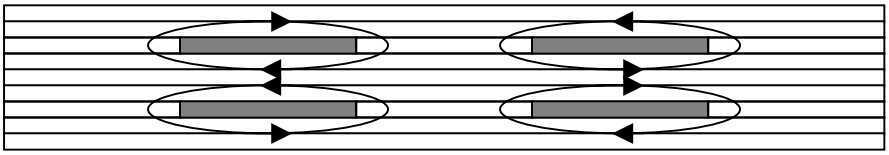

Figure [14c] Magnetic fields in a square wave coil structure.

Other coil structures were attempted, however, due to processing limitations, these structures failed during production.

2.) Sample production

Three series of test samples were produced using standard thick film screen-printing techniques. The materials used were selected from a low temperature cofired ceramic (LTCC) system of ferrite and silver pastes available from Heraeus Cermalloy, Inc. This system was chosen for its wide range of magnetic properties, and its ability to be easily processed into the structures under investigation. The production process may be summarized by the following sequence. First, an alumina substrate was mounted beneath a stainless steel mesh screen. The screen had been patterned by the use of a photo-imaged polymer mask. Second, paste (containing ferrite or silver particles) was deposited onto the screen then forced through the mask and onto the substrate by the action of a squeegee. Finally, the wet printed pattern was heat treated to dry the paste, burn out the polymer binders, and to

sinter the solid particles together. Successive printing steps using different materials and different patterns produced complex, three-dimensional structures.

3.) Measuring procedure

The primary tool for electromagnetic characterization was an impedance analyzer. To measure inductance, the analyzer sends a low current (5 mA), signal over a user defined frequency range through the test inductor. It then measures the impedance by comparing the return signal with the transmitted signal.

The impedance analyzer has no method, however, to vary the magnitude of the current of the test signal. Since one of the goals of this research was to characterize and improve saturation current, a method was needed wherein a variable current could be applied to the test inductor which would drive the saturation effect, while at the same time allowed the measuring of changes in inductance. It was proposed[27] to build the test apparatus of Figure [15]. In this system, a variable DC current source is placed in parallel with the impedance analyzer. A capacitor protects the impedance analyzer from the relatively high DC current, while a large (~100 times larger than the test inductors) minimized the current sharing of the AC signal through the loop parallel to the test inductor. This arrangement allowed the monitoring of inductance with a changing current. In this way, saturation current could be measured.

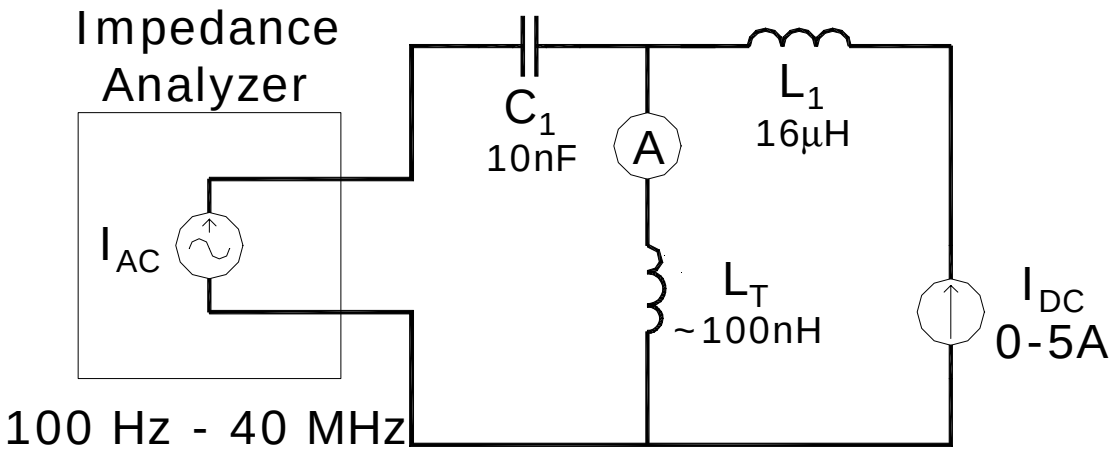

Figure [14] Schematic representation of measurement apparatus. The above circuit allows measurement of inductance while varying current.

A test circuit was designed and constructed in accordance with Figure [15]. The test circuit was connected to the impedance analyzer, and test inductors were mounted on the test circuit. Before each inductor was measured, the impedance of the test apparatus was measured using a straight conductive trace between the electrodes, and then subtracted from the gross impedance measured when the test inductors were installed. Initially, the current source was set at zero applied current, and a low current, "nominal" inductance was measured for the test inductor. Saturation current is commercially defined as the current that results in a 30% decrease from nominal inductance. Therefore, a value corresponding to 70% of the nominal inductance, termed the "saturation inductance", was calculated. Current from the DC current source was increased slowly until the measured inductance, which was being continuously scanned, reached the saturation inductance. The current, as measured by the in-line multimeter, was recorded as the saturation current.

Some sources of errors existed in the measurement setup, however. The most significant error was in the actual current distribution within the conductors. For the most accurate measurement, it is desirable that all of the current be subject to the uneven current distribution observed at high frequencies. In this test apparatus, however, the bulk of the current is DC and is, theoretically, homogeneously distributed throughout the conductor, while only a small fraction is operating at a high frequency. The result of this experimental error is to reduce the effects of current distribution.

If the inductance could be measured with both a variable current and variable frequency signal, the observed changes produced by the magnetic composite core structure would be much more significant. Another potential error arose from the parasitic inductance and capacitance of the test apparatus itself. This error was minimized by subtracting the measured impedance of the test apparatus from the observed measurements of the test inductors, which yielded the inductance value of only the test inductor. Another potential error lay in the low frequency resolution of the impedance analyzer. At low frequencies ($\omega < 500$ kHz), the inductance reported by the analyzer varies by values larger than the total inductance of the test inductors, however the resolution improved at higher frequencies. To minimize this error, measurements were taken at a frequency of 5.0MHz where the maximum observed variation in the short circuit inductance was approximately 5.0% of a typical test inductor.

To more accurately demonstrate the saturation effect at high frequencies, a test series was run wherein the inductance was measured as a function of frequency from 200 kHz to 40 MHz. A longer time averaging value was used to obtain more accurate data at low frequencies. As frequency was increased, the current distribution in the conductors was expected to continue to concentrate along the edges, thereby driving saturation in those regions. By measuring the change in inductance for a given substitutional method, the effect on reducing saturation can be estimated.

4.) Summary

In summary, test inductors were created using thick film screen-printing techniques with geometries that closely matched the geometries used in the finite element modeling. Electromagnetic measurements were also made that duplicated the conditions set in the finite element modeling. Improvements can be made to both the processing and measuring steps, however. The processing could be improved by more careful control of the drying step. Improper drying led to cracking in the multi-layered inductors. The measurement process could also be improved if measurements could be made using a signal with a user-defined frequency and current.

III. Chapter 3: Results

Variations in saturation current and inductance were measured for each series of substitutional strategies. Plots obtained from the analytical models are introduced to explain the experimental and finite element model observations. The results from both the modeled structures, and the measured test inductors are then summarized. The analytical modeling shows clearly that the permeability of a magnetic material varies with its location relative to the conductor and that optimizing the design of an electromagnetic device requires that more than one type of material be used. The finite element models indicate that certain substitution strategies improve inductance and reduce peak flux density, thereby reducing saturation. In the experimental results, varying the permeability in selected regions resulted in increases in saturation current, inductance, or both. In most cases, increasing saturation current resulted in decreasing inductance, and vice versa. In all the charts that follow, the dependent variable is the percent change in the measured quantity as compared to the experimental base line. The base line for comparison was a device constructed of a single magnetic material core with a permeability of 220.

Due to the constraints placed on the finite element analysis, and on the experimental devices that were manufactured for this research, the magnitudes of change for a given material substitution are small. The experimental devices for this research were large, relative to chip inductors or inductors on RFICs, utilized a material system with a limited range of permeabilities, compared to the range of permeabilities of all materials, and the test frequencies were low, compared to the GHz range of interest. The geometry, materials, and test frequencies were based on the available processes and measurement equipment. It is expected that for smaller inductors, utilizing a wider range of magnetic materials, and accurately tested at higher frequencies, the magnitudes of change will be greater for a given substitution method. The relatively small changes observed in this research serve as a “proof of concept” experiment, and can be extended to inductor designs where such changes will be more significant.

A. Analytical predictions

1.) Hysterisis loops

The first step in performing the analytical modeling was to obtain non-linear data from the materials that would be used to produce the test samples. These data were measured using a hysterisis graph using bulk samples obtained from the manufacturer. The bulk samples consisted of a toroid, pressed from the same ferrite material used in the ferrite paste. The toroids were wound with primary and secondary windings and connected to the hysterisis graph. The magnetic flux density (B) is measured as a function of applied magnetic field (H) by applying a sinusoidal current signal to the primary windings. The current induced in the secondary windings is measured to calculate the result. Table[1] below gives typical dimensions and winding parameters for these samples. Figure[16] shows the family of hysterisis loops for the materials under investigation.

Table [1] Typical parameters for bulk toroids used in hysterisis graph.

Thickness	2.0 mm
Width	4.0 mm
Magnetic Path Length	50 mm
Primary Turns	40
Secondary Turns	40

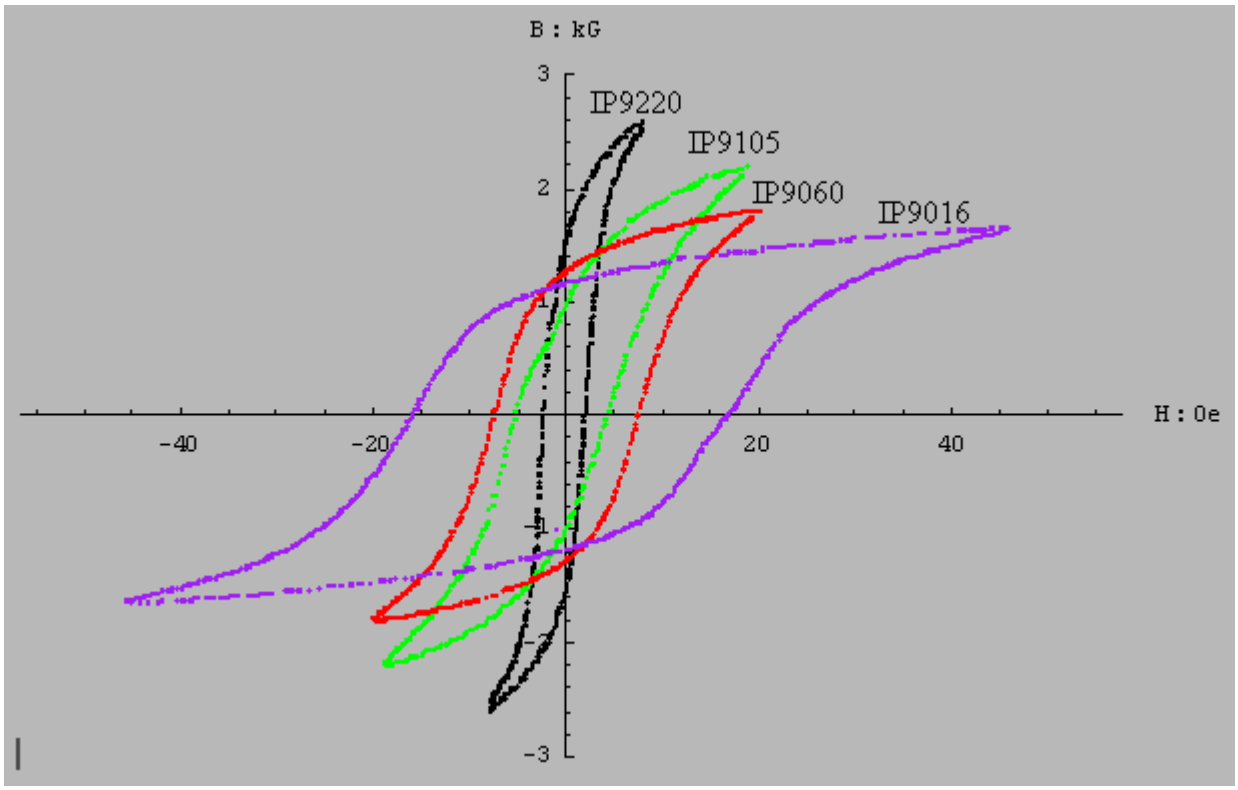

Figure [15] Hysterisis graph data for the ferrite materials under investigation.

2.) BH curves

The initial magnetization curves were estimated from the full hysterisis loops. Individual data points were obtained and plotted using Mathematica™. From these curves, the incremental permeability, μ, was obtained by taking the first derivative of the BH curve since

$$\mu = \frac{dB}{dH} \qquad \text{Eq.[10]}$$

From the above relationship and the non-linear nature of the BH curve, it can be seen that the permeability, and hence the electromagnetic performance, of a material is dependent on the applied magnetic field intensity. Figure[5] shows the initial magnetization (BH) curves for the materials in use.

It is important to note that the permeability reported for a given material is typically given as a single value, and not as a function of its environment. The reported permeability is determined by calculating the slope of a line drawn from the origin and tangent to the initial magnetization curve. This assumes a linear behavior of the material, and ignores local saturation effects due to high magnetic field intensities. In this research, the non-linear effects are considered and exploited to optimize the design of small-scale electromagnetic devices.

3.) Permeability as a function of magnetic field intensity

Plotting the incremental permeability vs. the applied magnetic field intensity shows that each material exhibits a maximum permeability at a different magnetic field intensity. Figure[6] shows this graphically. Note that for high H fields, the incremental permeability of classically high permeability materials is actually lower than for classically low permeability materials. This implies that if a region in the core is likely to exceed a certain value of H for most of its operation, then the performance of that device may be optimized by selectively placing “low” permeability materials in those regions. For example, if a “high” permeability material is used uniformly in an inductor where, due to its small size, the magnetic field intensity is sufficient to saturate the material, then the inductance will actually be lower than if a “low” but unsaturated material was used. If the geometry of the inductor is such that both high and low magnetic field intensities exist, then it becomes beneficial to use two or more different magnetic materials.

4.) Permeability as a function of path length

To illustrate the effect of geometry, consider a surface-mount chip inductor. These devices are commercially available in size 0805 chips from AVX Inc. Figure[17] shows a diagram of the package and coil geometry.

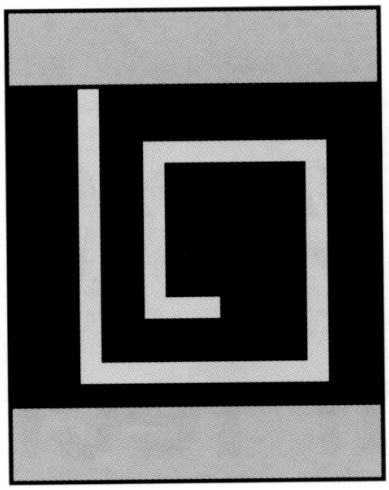

Figure [16] Diagram of size 0805 surface mount chip inductor.

From this diagram, the magnetic path length, l, is estimated to be from 0.2 to 0.4mm and these inductors are rated, based on thermal performance, at 500mA to 2000mA. For these rated currents, the magnetic field intensity, H, is calculated as a function of magnetic path length which is proportional to the distance away from the conductor, r, according to Eq[13] and plotted in Figure[18].

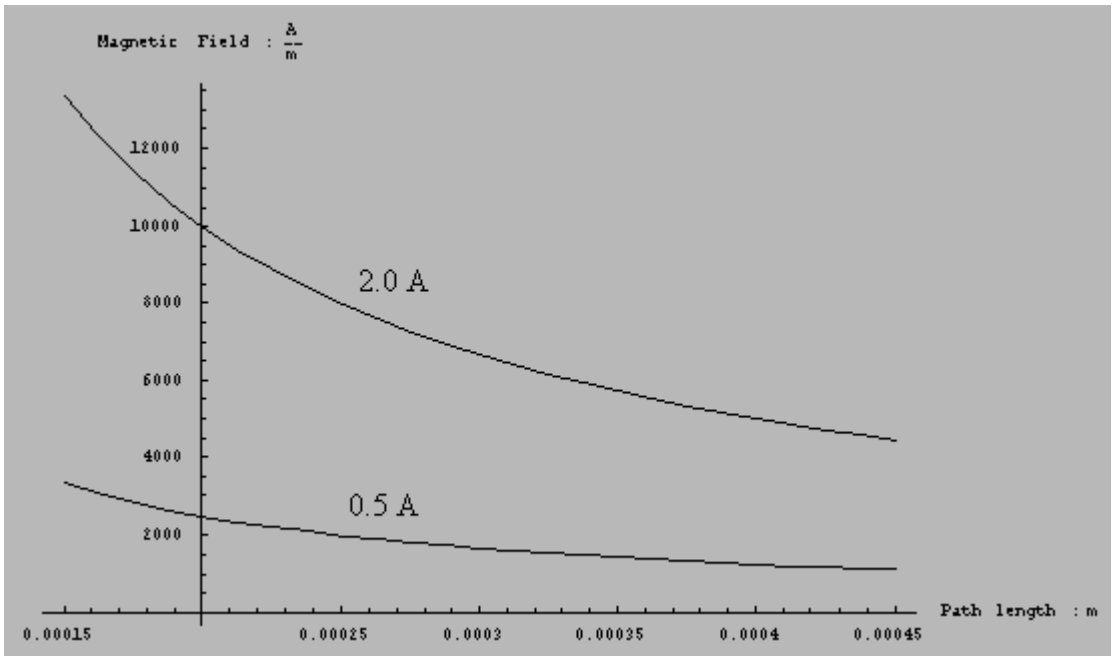

Figure [17] Magnetic field intensity, H, as a function of magnetic path length for selected currents.

From the plot, it is apparent that in these commercial devices, the magnetic materials used in this research would be saturated in certain regions in the core. These chip inductors, therefore, can be optimized by the application of a magnetic composite core approach.

5.) Summary of analytical prediction

The preceding explanation of the magnetic composite approach is used to clearly illustrate the need to consider the non-linear effects in a material when applied to small magnetic devices. It has been shown that the incremental permeability of a material is non-linear and varies with the applied magnetic field. The magnetic field varies with the distance away from the conductor and the current being carried in that conductor. Therefore, the magnetic properties of a material, especially permeability, vary with its location in a magnetic core. Applying this principle can be used to optimize the performance of small inductors and other electromagnetic devices.

B. Finite element modeling

1.) Observations of flux distribution

It has been found, using finite element modeling, that the careful placement of core materials with differing magnetic properties produces magnetic flux redistribution in the core and can improve the performance of thick film planar inductors.

a.) Early DC models

Two-dimensional models were initially constructed to simulate a parallel spiral core structure as previously described. A magnetostatic simulation was performed that gave a flux distribution based on an applied DC current. As can be seen in Figure[19] and [20], the flux distribution is nearly uniform above and below the conductors for the RL structure, and between the top and bottom conductors for the RR structure.

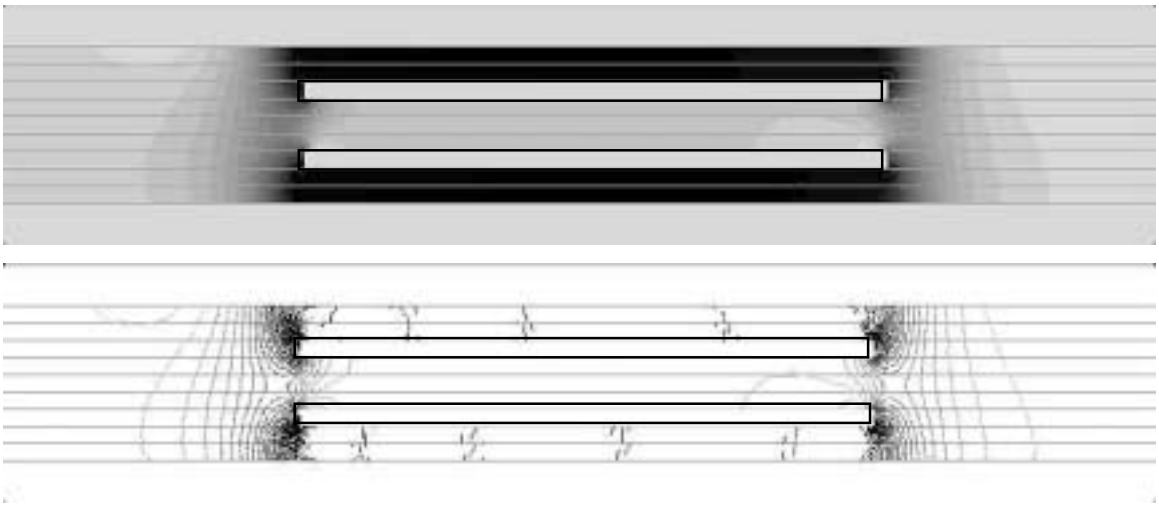

Figure [18] Flux distribution for a magnetostatic model. This is a RL structure. Note the level of coupling between the top and bottom conductors.

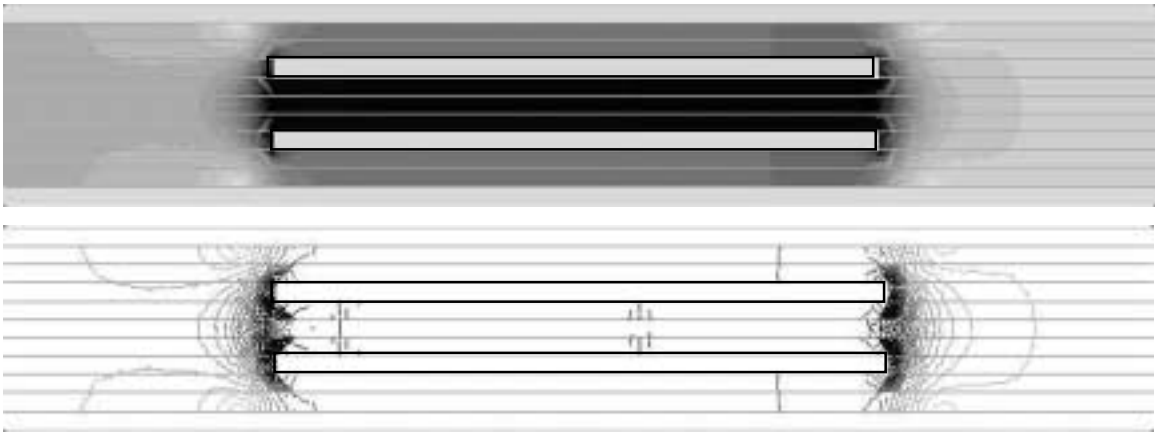

Figure [19] Flux distribution for a magnetostatic model. This is a RR structure. Note the high magnetic field between the conductors.

b.) Eddy current models

As the frequency is increased to 2.0MHz, the magnetic flux density increased along the edges of the conductors, and decreased in the region between the conductors. Figure[21] shows the flux distribution for a core with a single permeability of $\mu = 220$ at a frequency of 2.0 MHz. The uneven current distribution in the core material leads to inefficient use of materials located far from the

conductors, and saturation close to the conductors. Future models attempted to redistribute the flux more evenly, and thereby improve the volumetric performance of the core material.

Figure [20] Flux distribution at 2.0 MHz for a single material core, $\mu = 220$.

2.) Current distribution

a.) Causes of current crowding

The concentration of magnetic flux along the conductor edges is due to the non-homogeneous current distribution in the conductors, which is due to the skin effect and proximity effect at high frequencies and the proximity of the conductors to one another. Figure[22] graphically shows the current distribution across a conductor, and gives some numerical values for the percent difference in current density across the conductor.

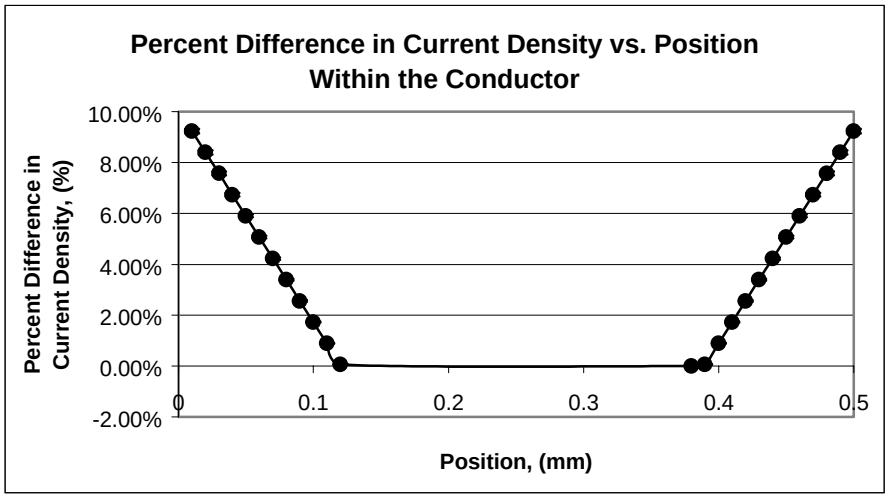

Figure [21] Percent difference in current density across a conductive trace at 2.0 MHz. Conductors in the model are 0.5mm wide.

3.) Linear materials in eddy current models

a.) Linear materials in eddy current models

Three basic substitutional methods were analyzed using eddy current modeling: 1) substitution of low permeability into the layers immediately above and below the conductors (Cladding Layers), 2) substitution of low permeability into the same layer as the conductor (Transmission line layers), and 3) substituting into the layer directly between the two parallel conducting coils (Separating layer). Figure[11] illustrates these substitution methods.

b.) Numerical results (saturation, inductance)

Models were run wherein the frequency was held constant at 2.0 MHz. Current was set at 1.0 A. The inductance was calculated for each modeled inductor using a field-level approach. The permeability of the materials in the cladding, separating, and transmission line planes was varied and inductance was calculated. Inductance varied with the substituted permeability in three different modes, depending on the substitution method. Substitution into the separating plane had little effect on the calculated inductance. Substituting low permeability into the transmission line layer increased the calculated inductance until a non-magnetic material was placed in this region. Finally, substituting low permeability material into the cladding layer resulted in a significant decrease in inductance. Figure[23] shows a graph of these modeled results. The mechanisms for these variations will be discussed later.

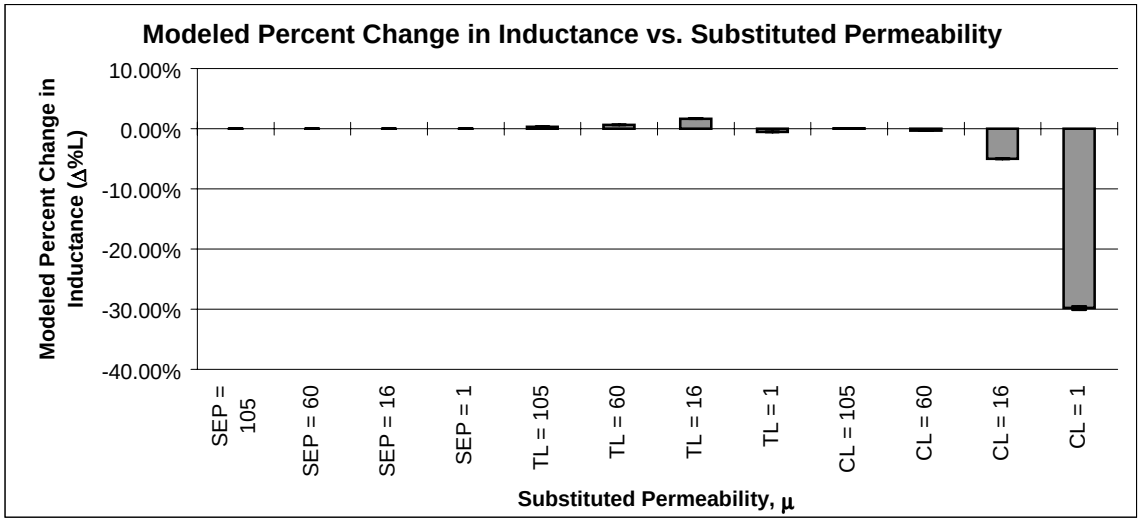

Figure [22] Modeled changes in inductance for parallel square-wave coil structure. "SEP" means that the low permeability material was substituted into the separating layer, "TL" designates a substitution into the conducting, or transmission line layer, and "CL" indicates a substitution made in the cladding layer.

Anther parameter of interest was the saturation current. The software used had no way of predicting saturation in an eddy current model, therefore, the peak flux density within the core was calculated and was initially thought to be a predictor of saturation current. It was hypothesized that as peak flux density decreased, the saturation current would increase. It will be shown later that this assumption was too simplified and that other mechanisms needed to be considered. Figure[24] shows a summary of the modeled peak flux density as a function of substituted permeability and structure.

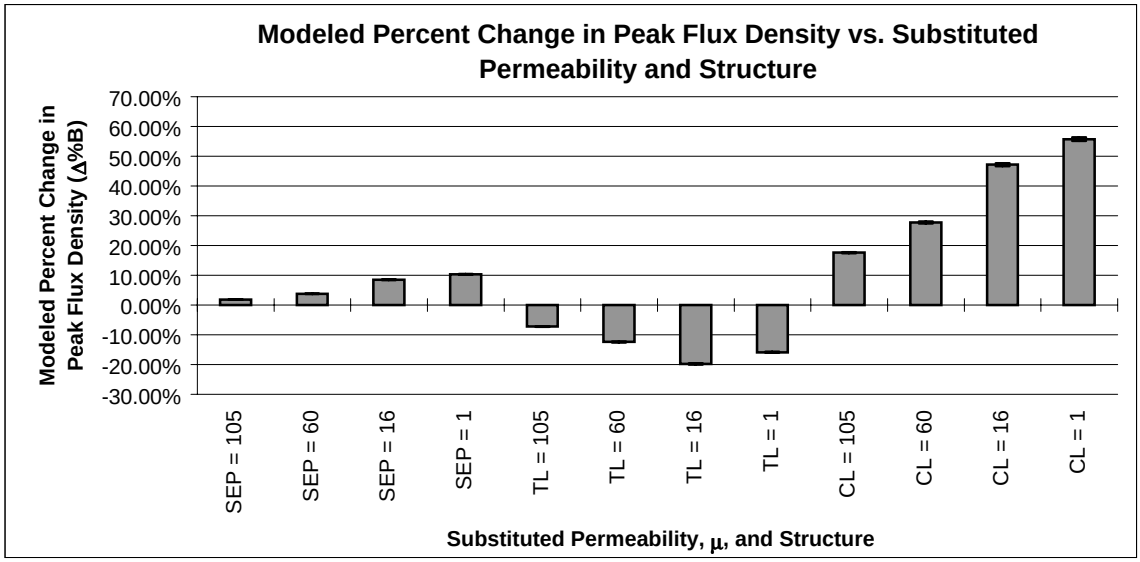

Figure [23] Modeled percent change in peak flux density for several substituted permeabilities. This model was based on a RL parallel circular spiral structure. As in the figure above, "SEP" means that the low permeability material was substituted into the separating layer, "TL" designates a substitution into the conducting, or transmission line layer, and "CL" indicates a substitution made in the cladding layer.

4.) Non-linear materials in magnetostatic models

a.) Non-linear materials in magnetostatic models

One of the deficiencies in the eddy current models is that they assumed that all the materials were linear and had a constant permeability. This assumption, by definition, does not allow a real prediction of saturation current. To predict saturation, magnetostatic models were created using non-linear material characteristics. A comprehensive series of models was run to find the relationship between substituted permeability and saturation current. Models were run using a "right-right", and "right-left" coil structure. In the "right-right" structure, two identical, right-handed coils were constructed parallel to one another so that the current flowing in the top coils was traveling in the opposite direction as in the bottom coil. In the "right-left" structure, the current flowing in both the top and bottom coils traveled in the same direction.

b.) Numerical results (saturation, inductance)

Figures [25] and [26] below show the numerical results of this modeling. From the graphs, it can be seen that the change in saturation current for the "right-right" coil structure is very minor, while the change in a "right-left" structure is on the order of 10%.

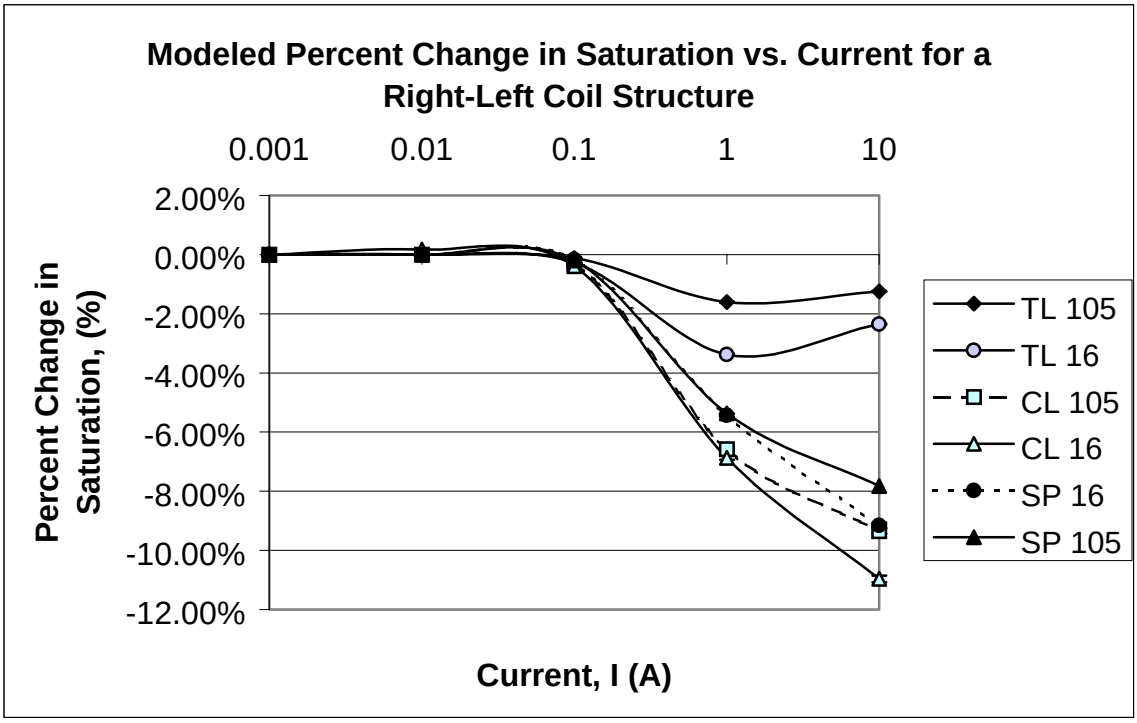

Figure [24] Percent change in saturation for currents of 1.0 mA to 10 A, DC, in a RL coil strucure.

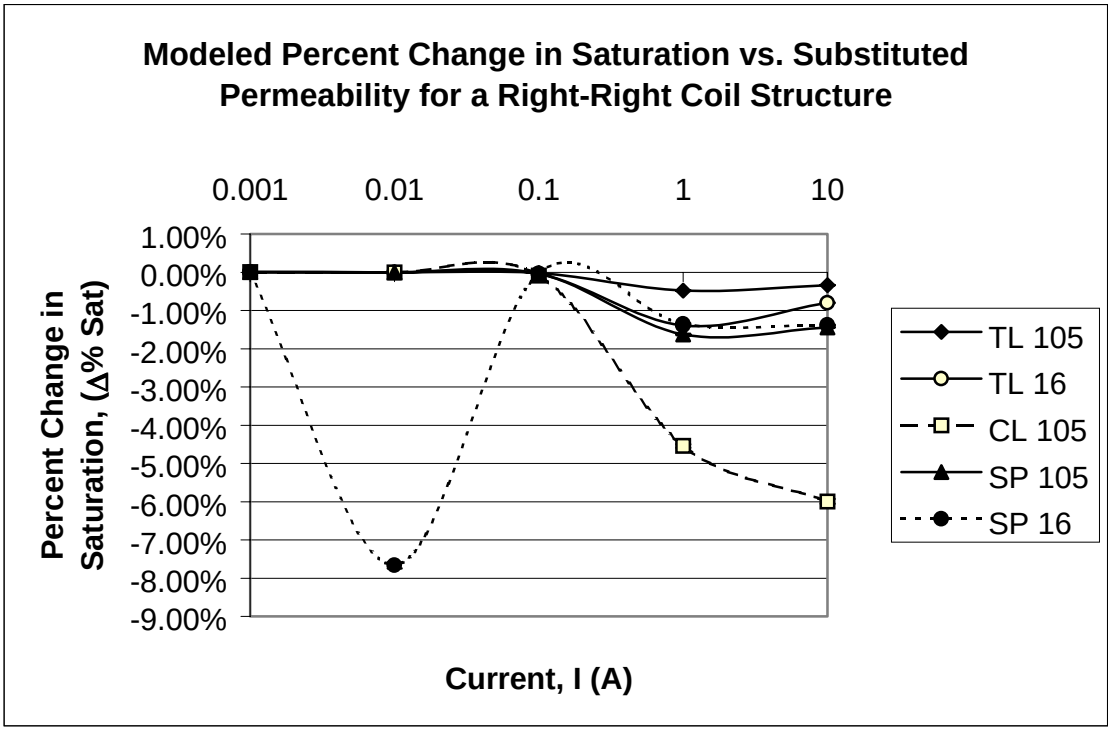

Figure [25] Percent change in saturation for currents of 1.0mA to 10A, DC, in a RR coil structure. There appears to be an anomalous data point at 0.01 A, for the SP 16 series.

The reason for this difference will be covered in the discussion. It should be noted, however, that the "right-right" coils were inherently less saturated than the "right-left" coils. Figure [27] compares the saturation of the two different coil structures holding all other variables constant.

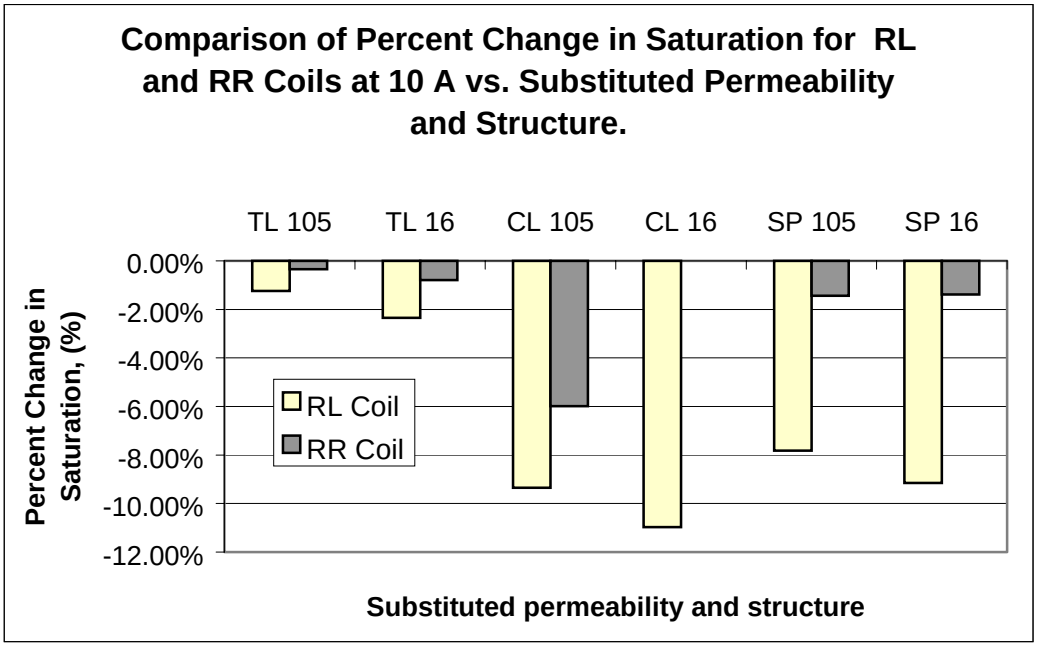

Figure [26] Comparison of the effect of material substitutions on RR and RL coil structures. Current for these models was 10.0 A, DC.

Inductance was also calculated for the magnetostatic models. The magnetostatic models, which do not account for frequency-dependent current distribution in the conductors, predicted that inductance would decrease for all substitutional methods. Figures [28] and [29] below show the percent change in inductance for the RR and RL coil structures vs. current.

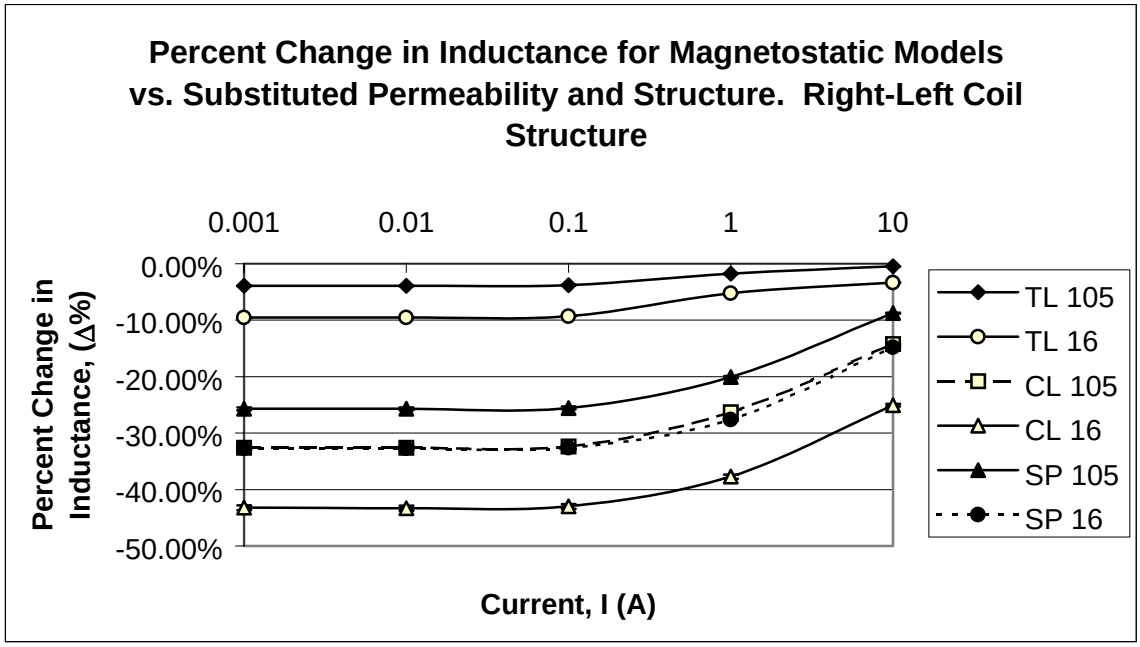

Figure [27] Percent change in modeled inductance for RL coil structures over a range of currents.

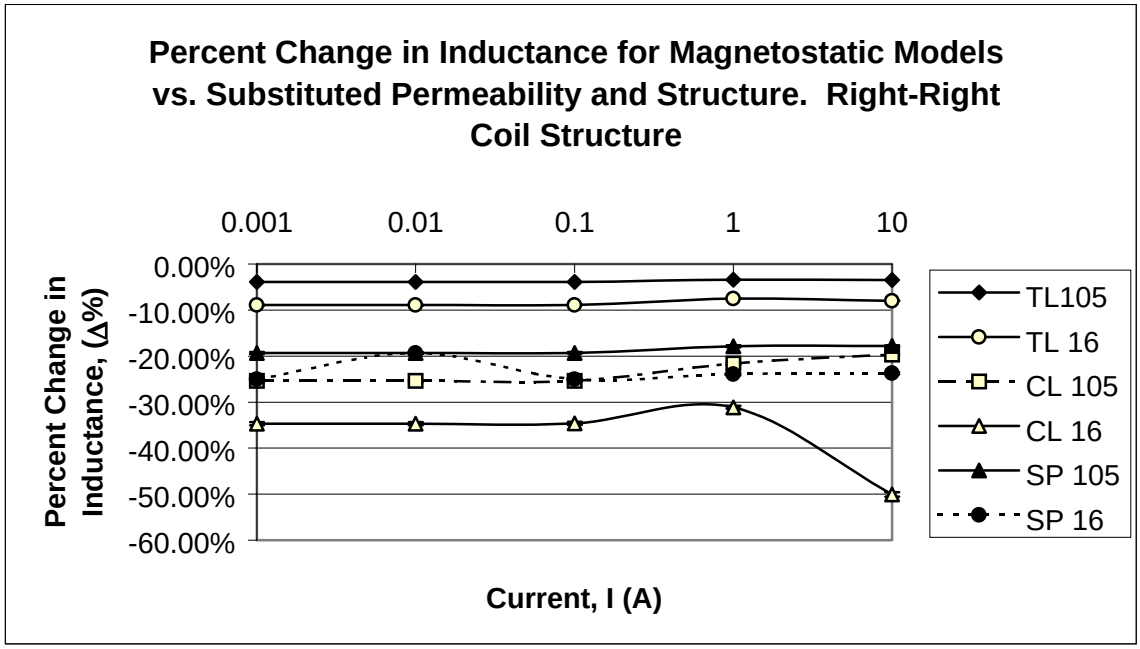

Figure [28] Percent change in modeled inductance for RR coil structures over a range of currents.

The magnetostatic models produce flux distributions very different from the eddy current models as can be seen in Figures[30], [31], and [32] below. While the magnetostatic models utilized non-linear material properties, they ignored the effects of an alternating current signal in the conductors.

[a] [b]

Figure [30] Permeability of $\mu = 16$ substituted into transmission line plane. [a] Frequency = 2.0 MHz, [b] Frequency = 0.0 MHz.

[a] [b]

Figure [31] Permeability of $\mu = 16$ substituted into cladding plane. [a] Frequency = 2.0 MHz, [b] Frequency = 0.0 MHz.

[a] [b]

Figure [32] Permeability of $\mu = 16$ substituted into separating plane. [a] Frequency = 2.0 MHz, [b] Frequency = 0.0 MHz.

5.) Composite models

a.) Creating the models (summary)

In an attempt to address the shortcomings of each of the previously described models, a series of "composite" models were constructed wherein a current distribution was simulated using a series of elements, each carrying a different DC current density.

b.) Flux distribution

Figures [33], [34], [35], and [36] below shows the flux distribution for some of the composite models created. The flux distribution for these models was similar to that of the magnetostatic models, but gave insight into the flux distribution within a non-linear magnetic core. Graphically, it can be seen that substituting low permeability material into the cladding and separating layers redistributes the flux between conductors in the same plane, thereby lowering the peak flux density.

Figure [33] Composite model with a single material core, with a permeability of $\mu = 220$.

Figure [34] Composite model with a permeability of μ = 16 substituted into the TL layer.

Figure [35] Composite model with a permeability of μ = 16 substituted into the CL layer.

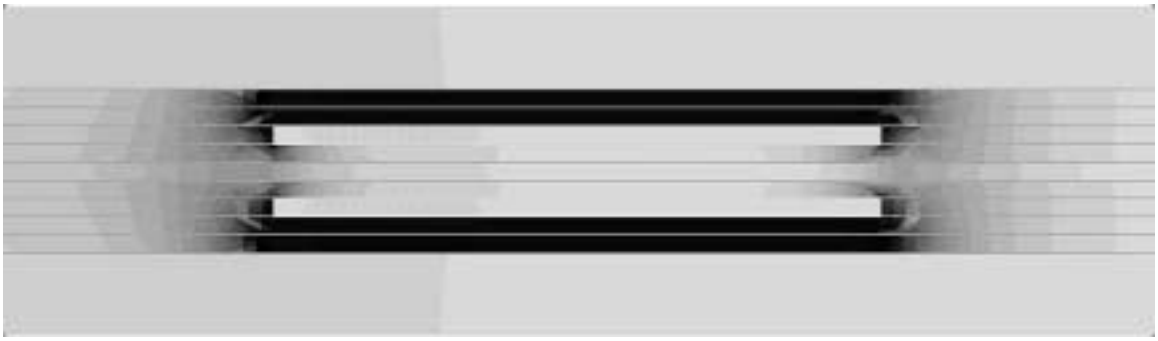

Figure [36] Composite model with a permeability of μ = 16 substituted into the SP layer.

c.) Numerical results (saturation, inductance)

The output generated by these composite models consisted of a square matrix describing the mutual inductance between each of the conducting elements. The self-inductance of the device is

calculated by summing the diagonal of the matrix. On the previous models, calculating the self-inductance was easily accomplished using a spreadsheet. The composite matrices, however, contained 450 rows and 450 columns, making the calculation of inductance and saturation currents extremely difficult. These calculations, therefore, were not completed.

6.) Summary of finite element modeling

The modeling software used allowed the calculation of inductance either integrated along a line, or rotated about a central axis. For our purposes, it was not necessary to calculate the total inductance, but rather the change in inductance to determine the relative effects of a particular design modification. The modeling predicted very little changes in self-inductance, except in the instances where substitutions of very low permeability materials were made in the cladding layers. Increases in inductance were predicted for several substituted permeabilities in the transmission line plane. Figure [37] contains actual modeled inductance values, while Figure [23] displays relative changes from the baseline.

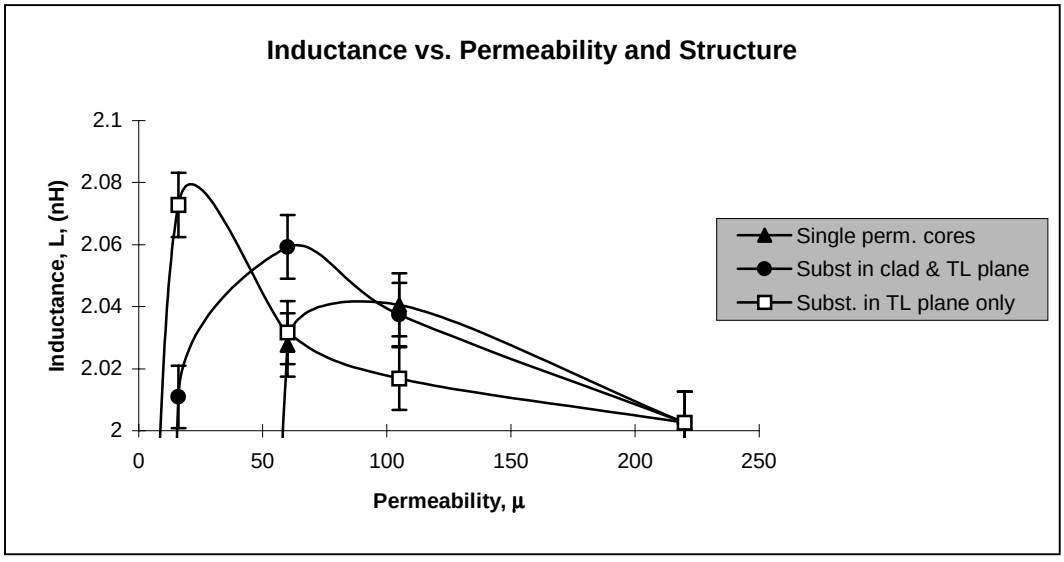

Figure [37] Modeled values of total inductance for selected structures.

In the substitutional series where the low permeability was substituted into the separating layers, there was little if any predicted change in self-inductance. For substitutions made in the transmission line planes, denoted "TL", a peak positive change was predicted for a permeability of $\mu = 16$. The importance of this observation will be explained below. When substitutions were made in the cladding layers, labeled "CL", little variation was predicted until very low permeability materials were used, at which point there was a large decrease in predicted inductance.

Since the saturation characteristics of the ferrite pastes were not available in the beginning, the modeling software could not be used to predict saturation currents. Instead, peak magnetic flux density was used as a predictor of saturation current. It was assumed that reducing peak flux density would reduce the effect of saturation, and the saturation current would increase. Figure [38] shows relative percent changes in peak flux density for the various substitutional methods.

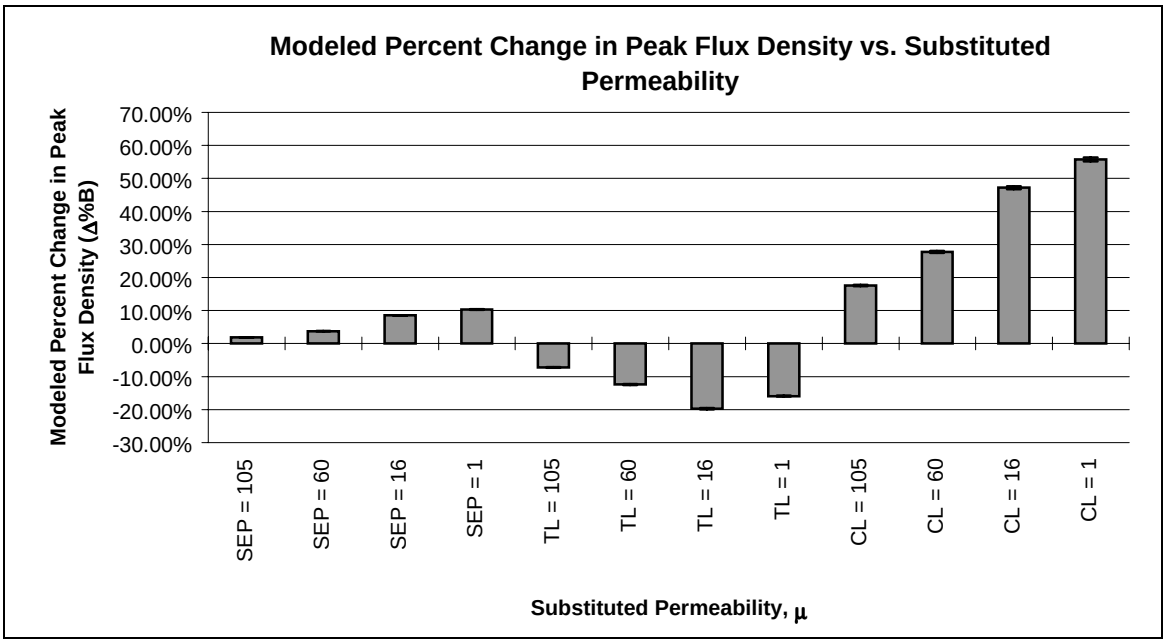

Figure [38] Percent change in peak flux density, as compared to baseline model, for several substitutional methods.

A similar trend analysis can be used as is described above. For substitutions in the separating layers and in the cladding layers, there was a steady increase in predicted flux density as permeability was lowered. For transmission line plane substitutions, lowering permeability resulted in lower peak flux densities.

C. Experimental verification

1.) Inductance

Early inductance values were measured for the square wave structure over a wide range of currents and frequencies. It was determined that measurements below 1.0MHz contained too much variance, and were considered not useful. Measurements taken between 5.0 MHz and 40 MHz showed very little (~5%) variance over the entire frequency range. The reason for this observation will be explained in the discussion. Figure [39] shows the change in inductance for various substitutional methods at 5.0 MHz. On selected samples, inductance values for intermediate currents below I_{sat} were measured and plotted to show the change in inductance as current increases. Figure [40] contains these plots.

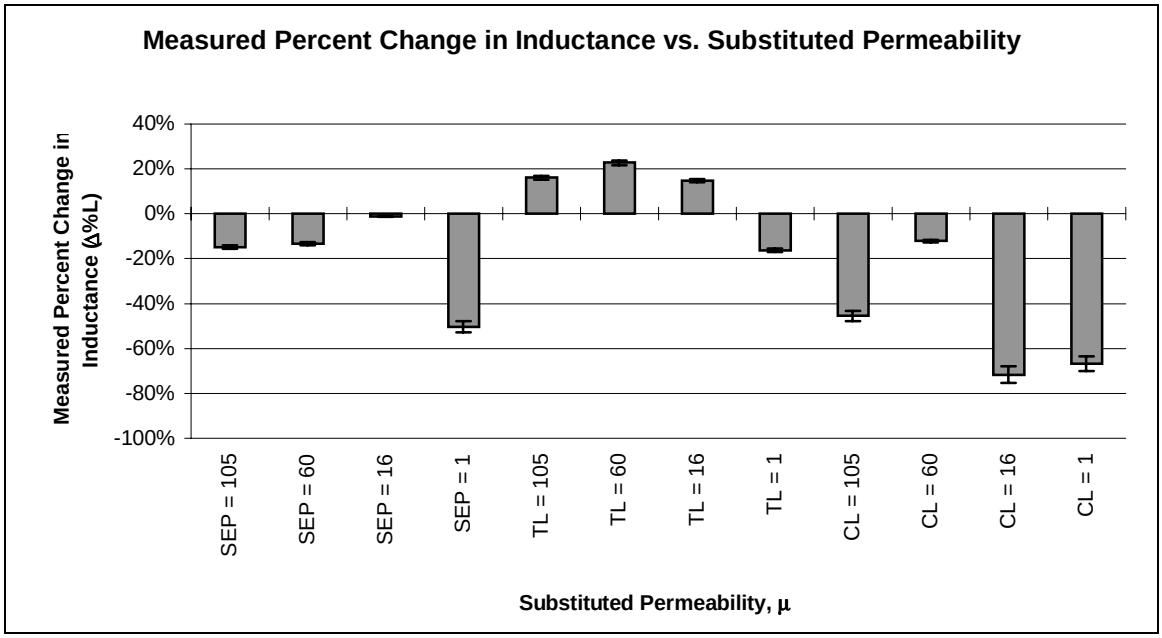

Figure [39] Measured percent change in inductance vs. substituted permeability.

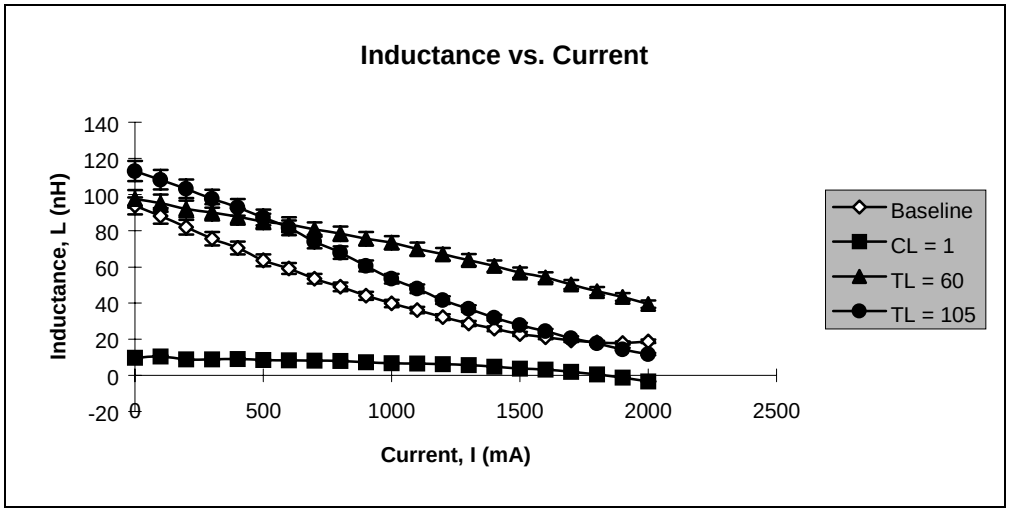

Figure [40] Measured inductance vs. applied current for selected structures.

Inductance values varied widely over the different substitutional methods. For substitutions made in the separating plane, denoted by "Sep" along the x-axis, induction decreases as permeability decreases. The sample wherein a permeability of $\mu = 16$ must be disregarded as an erroneous sample. In the series where low permeability materials were substituted into the transmission line planes, denoted "TL", there is a maximum value at $\mu = 60$. The importance of this observation will be explained below. Finally, the cladding layer substitutional method, denoted "CL" resulted in negative departures from baseline for all permeabilities.

Another series of measurements was made on a flat, circular spiral coil. This structure consisted of a single coil instead of two parallel coils. Devices with parallel coils were constructed but failed during processing. The measuring techniques were refined to allow measurements down to 200 kHz with high precision (+/- 0.1%). For this series of measurements, current was held constant at approximately 5.0mA and frequency was varied from 200 kHz to 40 MHz. Figure[41] below, gives the inductance values measured over this range.

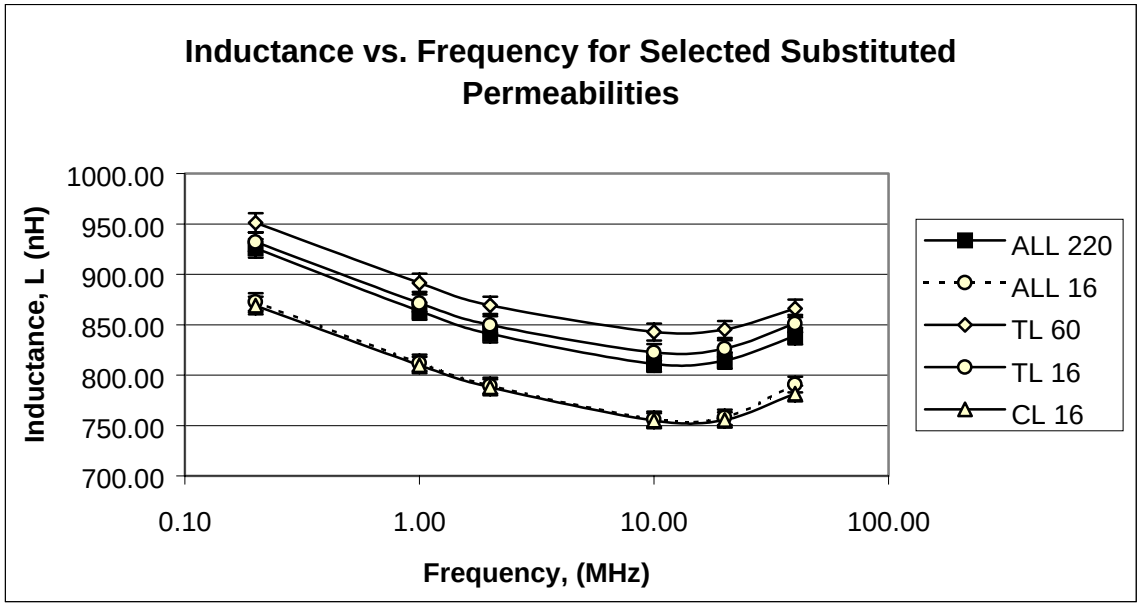

Figure [41] Measured inductance over a range of frequencies for single coil, circular spiral inductors.

It can be seen from this graph that substituting low permeability materials into selected regions improved the inductance by approximately 1% to 4%. To more clearly observe the effects of making material substitutions, the percent change in inductance is plotted vs. frequency in Figure [42].

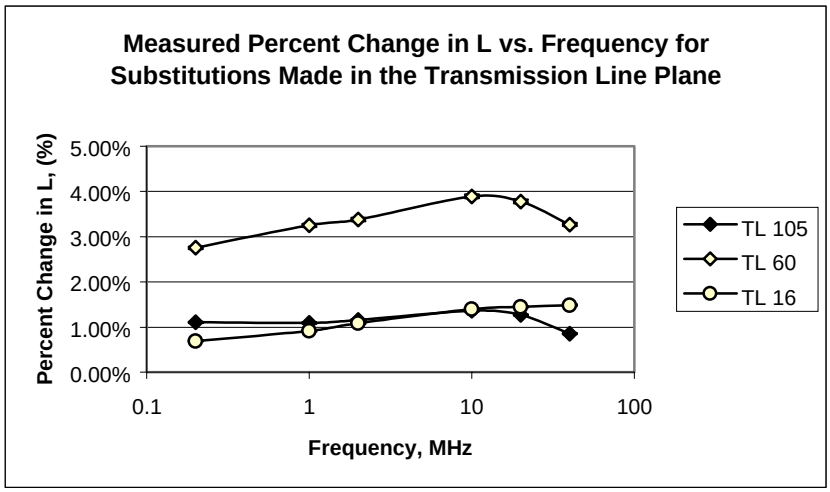

Figure [42] Measured inductance over a range of frequencies for single coil, circular spiral inductors.

It can now be seen that substituting a low permeability in the transmission line plane not only improves inductance, but the improvement increases as frequency, and hence current crowding, increases. Some of the possible reasons for this will be covered in the discussion.

2.) Saturation current

Saturation current is commercially defined as the current required to reduce the nominal inductance by 30%. The measurement for saturation current, therefore, is partially dependent on the accurate measurement of inductance. Figure [43] gives the percent changes in saturation current for various substitutional methods while total saturation currents are listed on Table [2]. These measurements were made on parallel square wave coil inductors. Temperature was measured on selected samples while DC current was applied. The average temperature, as measured by an off-contact laser thermometer, was approximately 60 ^{o}C, with 1500 mA of current, at room temperature, with no heat sink or forced air-cooling.

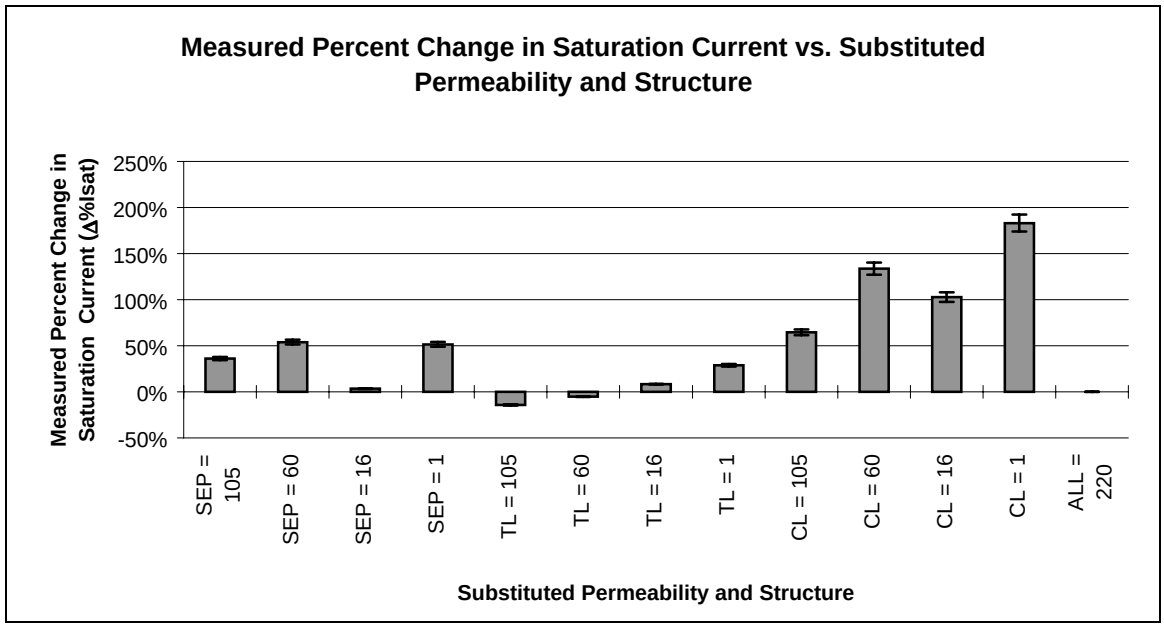

Figure [43] Measured percent change in saturation current vs. substituted permeability.

Table [2] Saturation current vs. substituted permeability.

Permeability	I_{sat}, mA
SEP = 105	993
SEP = 60	1124
SEP = 16	755
SEP = 1	1106
TL = 105	625
TL = 60	691
TL = 16	791
TL = 1	941
CL = 105	1201
CL = 60	1706
CL = 16	1481
CL = 1	2067
Baseline	730

The variation of saturation current over the range of substituted permeabilities followed more definable trends. In the separating plane substitution, there was little variation over the range of permeabilities, again discounting the sample where the permeability was $\mu = 16$. Over the transmission line substitution, a steady increase in saturation current was observed for decreasing permeabilities. Finally, in the cladding layer substitution, a very large increase in saturation current was observed.

The results for the saturation current do not completely represent the saturation current for a device in a real system. The reason for this lies in the measurement apparatus. The schematic of the measurement apparatus is shown in Figure [15]. Electrically, this technique allows a variable current DC signal to be overlapped with the variable frequency signal from the impedance analyzer. The result is shown in Figure [44].

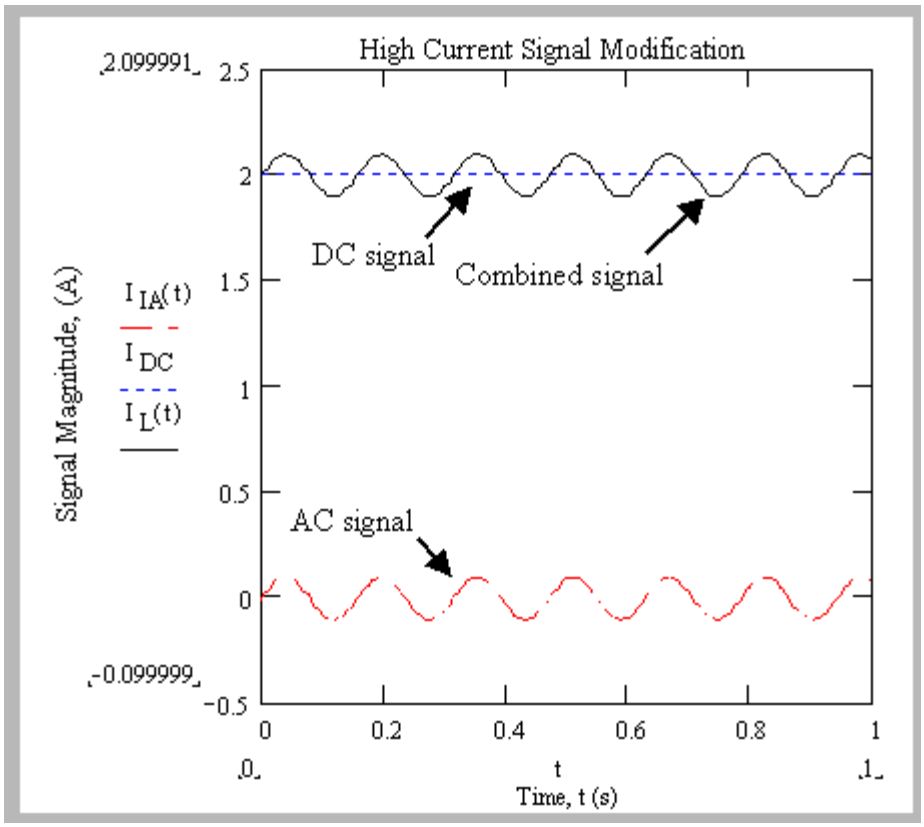

Figure [44] Schematic representation of test signal applied to test inductors.

This system has a deficiency, however, in that the current distribution is not captured for all of the current. Current crowding is caused by the small, 5.0 mA signal only. The bulk of the current (1.0 A to 2.0A) is carried by the DC signal and is assumed to be uniformly distributed within the conductor. Therefore, the observed change in saturation current that should result from a redistribution of the magnetic flux is minimized. It is expected, therefore, that if the inductance and saturation current could be measured for a signal with variable frequency and variable current, the observed changes to saturation current would be much larger in magnitude.

3.) Summary of experimental verification

To summarize the measured results, two primary structures were measured. The first structure consisted of two “square wave” coils physically parallel to one another and electrically connected in series. Both inductance and saturation currents were measured for these devices. It was found that

the greatest increase in inductance came with substituting a permeability of $\mu = 60$ into the transmission line, while the highest increase in saturation current resulted from substituting a permeability of $\mu = 16$ into the cladding layers. The measured saturation current represents a composite current distribution within the conductors of a small, 5.0 mA 2.0 MHz signal overlapped with a variable current DC signal.

Inductance measurements were also made on flat, circular spiral inductors. These devices consisted of a single circular spiral conductor imbedded in a ferrite core. The test current was held constant at 5.0 mA while the frequency was varied from 200 kHz to 40 MHz. It was observed that substituting low permeability materials into selected regions improved inductance, and that the improvement increased with increasing frequency.

Due to the constraints placed on the finite element analysis, and on the experimental devices that were manufactured for this research, the magnitudes of change for a given material substitution are small. It is expected that for smaller inductors, utilizing a wider range of magnetic materials, and accurately tested at higher frequencies, the magnitudes of change will be greater for a given substitution method. The relatively small changes observed in this research serve as a "proof of concept" experiment, and can be extended to inductor designs where such changes will be more significant.

IV. Chapter 4: Discussion

A. Introduction

In the following section, the interpretation of the research data will be presented. Effects on saturation current and inductance will be analyzed in turn. In each case, the material will be presented in four steps. First, analytical predictions will be discussed using fundamental principles of electromagnetics. Analytical solutions will be presented that will predict the electromagnetic behavior for simplified geometries. Second, finite element analysis results for more complex structures will be discussed. Third, experimental evidence will be used to confirm or refute the analytical predictions or the finite element models. Finally, any discrepancies between these three results will be discussed. It will be shown that in some cases the initial assumptions were too simple to predict actual performance, but that fundamental principles of electromagnetics can be used to more carefully analyze the modeled data and to explain the measured results. More complete assumptions and explanations will be presented to describe the correlation between the computer models and the experimental results.

B. Variations in saturation current

1.) Introduction

Saturation is a result of a magnetic field applied to a material that is sufficient to align all of the magnetic domains parallel to the magnetic field. When this state occurs, application of a higher magnetic field intensity results in no further increase in the magnetic flux density (B), and, hence, the total magnetic flux contained in the material. To minimize saturation, the peak magnetic flux density in any region in the core material must be minimized. In the following section, it will be shown first that the saturation of a region of material is dependent on the distance of that region from the current-carrying conductor. It will further be shown that substituting classically low permeability materials into selected regions will increase the saturation current.

2.) Interpretation of experimental results using fundamental principles and computer models.

a.) Frequency dependence of saturation

i. Analytical prediction

Saturation current is clearly linked to the peak flux density in a region of non-linear magnetic material. Figure [45] presents a schematic B-H curve for such a material.

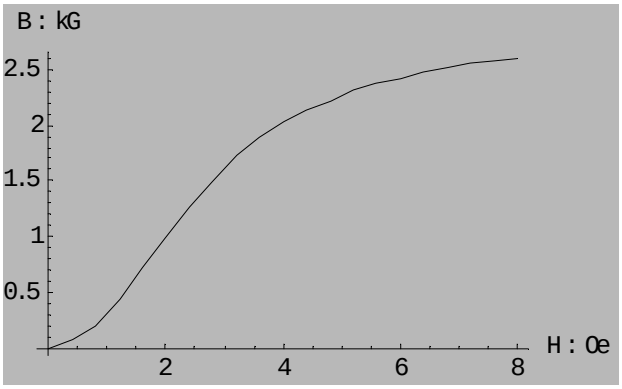

Figure [45] BH curve for a typical non-linear material under investigation.

As the applied current increases, so does the magnetic field intensity according to Maxwell's third equation:

$$\oint H \bullet dl = I \qquad \text{Eq.[2]}$$

Where:

H = magnetic field intensity l = magnetic path length I = current

The resulting flux density, **B**, produced in the material increases approximately linearly to a certain maximum value. Above this value, called the saturation magnetization (B_{sat}), further increases in magnetic field intensity result in no further increases in flux density. The incremental permeability

of a material is defined as the slope of the B-H curve. Because the self inductance of a current carrying conductor is dependent on permeability through:

$$L = \frac{d\Phi}{dI} \qquad \text{Eq.[4]}$$

and

$$\Phi = \int \mu \cdot HdA \qquad \text{Eq.[14]}$$

Where:

L = self inductance Φ = total magnetic flux I = applied current

μ = permeability H = magnetic field intensity A = cross sectional area

Then as the permeability decreases due to saturation effects, so does the inductance. It is this phenomenon that reduces the inductance at higher currents and leads to the definition of saturation current.

The simple assumption made in the early stages of modeling, that minimizing the peak flux density in the structure would necessarily lead to higher saturation currents, ignored possible secondary effects present in magnetic composite cores. The basic premise should be modified to include that minimizing flux density in a given region will minimize saturation only in that region.

If the current density in a current-carrying conductor at high frequencies is examined, it can be seen that the distribution is inhomogeneous and that the current will tend to crowd along the edges of the conductor. Current crowding, in turn, leads to an uneven magnetic flux distribution in the core material. The inhomogeneous current distribution in a conductor is caused by both the skin effect, which limits the penetration of an electromagnetic wave into a conductor, and the proximity effect, which seeks to minimize total stored energy by producing destructively interfering magnetic fields between conductors.

The skin depth of a material is given by:

$$\delta = \frac{c}{k\omega} \qquad \text{Eq.[3]}$$

Where:

δ = skin depth c = speed of light in vacuum ω = frequency

k = material constant

From this equation, it can be seen that for higher frequencies, the current will penetrate less into the conductor. For conductors that are non-circular in cross-section, the skin depth produces a higher current density along the edges of the conductor. The proximity effect contributes to the uneven current distribution by redistributing the current to minimize the stored energy, and thereby minimize the total energy of the system. Two high frequency conductors in proximity to one another will minimize energy by redistributing the current such as to produce destructively interfering magnetic fields between the conductors, reducing the net magnetic field. In the cross sections of printed conductors, which have a high aspect ratio, the concentration of current along the conductor edges produces the desired magnetic fields.

The above analytical expressions predict, then, that to minimize saturation in a high-frequency device, the high magnetic flux density that is produced due to current crowding must be redistributed to minimize the peak flux density in the high magnetic field regions.

ii. Finite element modeling

Possibly one of the greatest strengths of the finite element modeling is its ability to visualize the current distribution in a conductor, and the resulting magnetic flux distribution in the core material. Using the models, the current distribution was calculated for given frequencies. Substitution of low

permeability materials resulted in a redistribution of magnetic flux that could be easily visualized using the models.

Figure [22] contains a graph of the numerical values for the current density across a cross-section of a conductor carrying 1.0 A (rms) of current at 2.0 MHz obtained from a finite element model. Calculated current densities for given regions are obtained by defining a line through the conductor, then plotting the current densities that exist along that line. Graphically, we see the predicted current crowding along the edges of the conductor, and from the graph, we not that at 2.0 MHz, the difference from the edges to the center of the conductor is approximately 10%. As frequency increases, and as the distance between conductors decreases, the difference in current density will increase.

Using the equation:

$$I = \frac{H}{l} \qquad \text{Eq.[15]}$$

we see that as the current in a localized area increases, so must the magnetic field intensity. With increased magnetic field intensity, the magnetic flux density increases to the point of saturation.

Figure [7] shows the magnetic flux distribution in the vicinity of a conductor carrying a 1.0 A (rms) current at 2.0 MHz. In this model, the entire core is made of a single magnetic material having a permeability of $\mu = 220$. This model also assumes that the material behaves linearly for all magnetic field intensities. Note the concentration of magnetic flux in the regions along the edges of the conductors, and the lack of flux elsewhere. This model predicts that as the current increases, so will the flux densities of the regions near the edges of the conductors, leading to early saturation of these regions, while the areas far from the conductor edges contain relatively little magnetic flux.

If a material substitution could be made such that the magnetic field was forced into the regions far from the conductor edges, then for the same applied current, the effective magnetic path length

would increase, and thereby lower the peak flux density. Figures [30], [31], and [32] show three substitutional strategies wherein a non-magnetic material has been substituted into the cladding, conducting, and separating layers, respectively. As can be seen, the flux distribution, for the same current characteristics, is much different. When a non-magnetic material is substituted into the cladding layers, the magnetic field is concentrated in the region between the parallel conductors, as in a bulk toroid inductor. The peak flux density in this model is actually higher than in the homogeneous core. In the model where the non-magnetic material has been substituted into the conducting layer, the flux is redistributed into the regions between conductors in the same plane. This redistribution makes more efficient use of the material in those regions, and lowers the flux density. Substituting a non-magnetic material into the separating layer effectively isolates the top and bottom parallel coils, and increases the peak flux density.

Instead of inserting a non-magnetic material, a low-permeability ferrite can also be substituted. Substituting a low permeability ferrite has the advantage of allowing a more precise tailoring of the flux distribution, while retaining sufficient magnetic properties to yield a high inductance. Figures [46] (a), (b), and (c) show a progressively wider flux distribution as lower permeability materials are substituted into the conducting layer, while Figure [38] shows the modeled percent change in peak flux density vs. substituted permeability for the three substitutional strategies.

[a] $\mu = 220$ (All)

[b] μ = 105 (TL Plane)

[c] μ = 16 (TL Plane)

Figure [46] (a), (b), (c) Widening flux distribution as lower permeabilities are substituted into the TL plane.

It was desired to model the predicted trends in saturation current for devices made using non-linear materials. To accomplish this goal, models were constructed using experimentally obtained non-linear material properties. Current, in the models, was varied from 1.0 mA to 10.0 A, and the inductance was calculated. As current was increased, inductance decreased due to saturation in the high magnetic field regions. Figure [47] contains a graph of the percent change in saturation vs. substituted permeability and structure. In this graph, a negative percentage indicates that the structure is less saturated than a structure made from a single permeability (μ = 220) core.

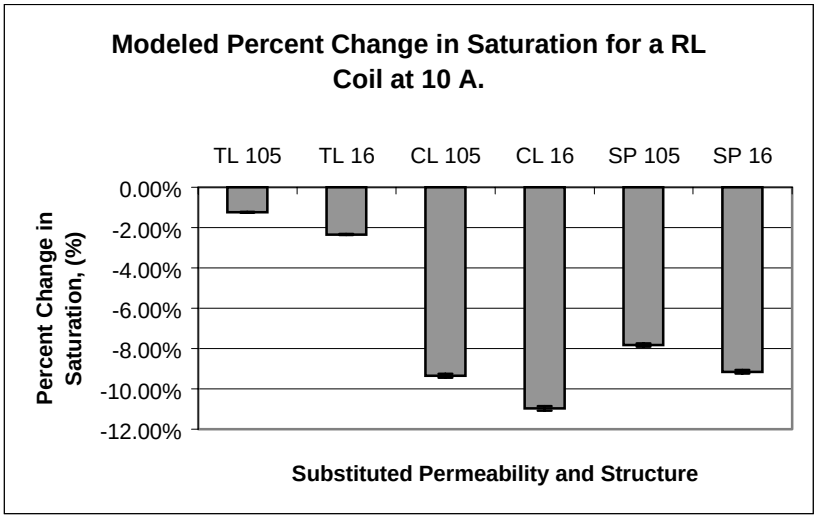

Figure [47] Percent change in saturation for selected substitutions and permeabilities. Results are given as a percent change in saturation compared to the baseline model.

From the graph, it can be seen that substitution in the cladding layers offers the greatest reduction in saturation. It will be shown later, however, that making substitutions into the conducting layers yields the best combination of saturation current and high inductance.

iii. Experimental verification

To determine the frequency dependence of saturation current, it would be necessary to measure inductance as a function of both current and frequency. For the saturation measurements made in this research, a large DC current was summed with a small AC signal. While this gave some measurement of saturation current, it did not allow for the measurement of saturation current as a function of frequency.

iv. Discrepancies

Discrepancies between modeled and measured saturation characteristics are due primarily to the inability of the modeling software to combine non-linear material properties with an AC signal. Measurement of the saturation current also contained errors in that the frequency and current could

not be arbitrarily varied. Improvement of the modeling and experimental techniques will reduce the differences between the modeled and experimental results.

b.) Peak flux density in the high permeability material

Since the mechanism for saturation in a magnetic material is tied to the peak flux density in that material, it is desired to be able to redistribute a given amount of total flux over a wider area and thereby minimize the flux density. The effects of flux redistribution can most easily be seen in the case where low permeability materials were substituted into the transmission line planes. Figure [46] shows, graphically, how reducing the permeability of these layers results in a redistribution of magnetic flux over a larger area, thus minimizing flux density.

From the models, we predict a reduction in peak flux density, Figure [48], and from experimental measurements, we observe a corresponding increase in saturation current.

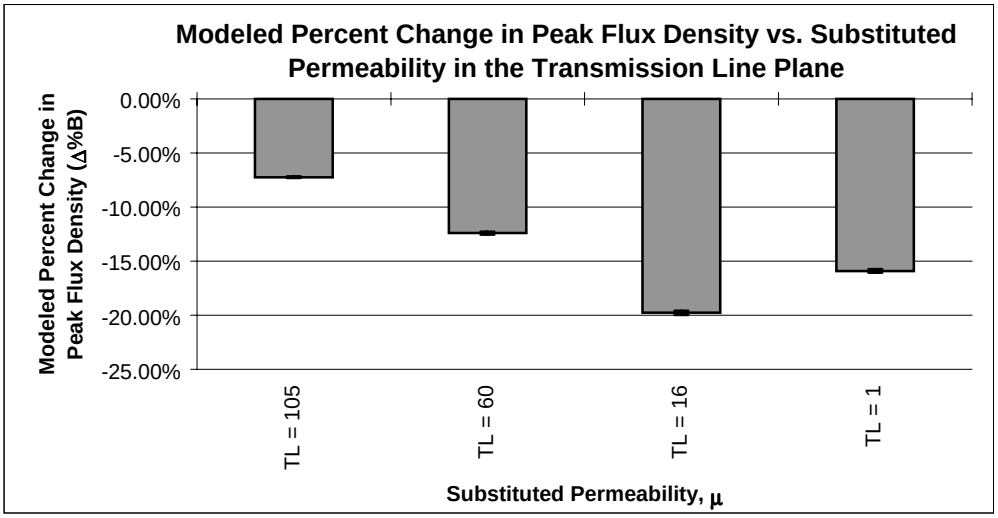

Figure [48] Modeled percent change in peak flux density vs. permeability substituted into the transmission line plane.

i. Analytical prediction

These data can be explained using the following relationship:

$$B = \mu \cdot H = \frac{\Phi}{A} \therefore A = \frac{\Phi}{\mu \cdot H} \qquad \text{Eq.[16]}$$

and

Maxwell's second equation:

$$\nabla \bullet B = 0 \qquad \text{Eq.[17]}$$

Where:

∇ = dell operator A = area through which magnetic flux "flows"

All other variables are defined above.

Maxwell's second equation simply states that magnetic flux does not radiate from any closed surface. From this equation, a fundamental property of electromagnetics is obtained: that the magnetic field flows in a circulating path about a current carrying conductor. Using the above relationship, Eq.[16], we see that the area (A) required to pass a given amount of magnetic flux (Φ) is inversely proportional to the permeability (μ) of the material. As the permeability is lowered, a larger cross sectional area is required to pass the magnetic flux. Also from Eq.[16], we note that increasing the cross sectional area, obviously, reduces the flux density which moves the material farther away from its saturation magnetization.

ii. Finite element modeling

Consider again the finite element models used to display the flux distribution throughout the core. If it were assumed that only reducing the peak flux density in the core would reduce saturation, then it would be predicted that substituting a low permeability material into the conducting layers would produce the highest saturation current. Figure [24] shows the modeled percent change in peak

flux density vs. substituted permeability and structure. Graphically, Figures [30], [31], and [32] we see that this form of substitution results in the most uniform flux distribution, whereas the other two methods seem to concentrate flux in different areas.

iii. Experimental verification

Test devices were constructed to test the above models. The printed inductors used for saturation measurements were of the "square-wave" type, see Figure [12] where two "square-wave" coils were printed parallel to one another and electrically connected in series. A test apparatus was used wherein a 2.0 MHz signal from an impedance analyzer measured inductance while a variable current DC signal, superimposed on the AC signal, was used to drive saturation.

The initial assumption was that the saturation current would be inversely proportional to the peak flux density in the core material. It was hypothesized that if peak flux density was reduced, the saturation current would increase. Figure [49] compares the modeled percent change in peak flux density vs. substituted permeability with the measured change in saturation current vs. substituted permeability.

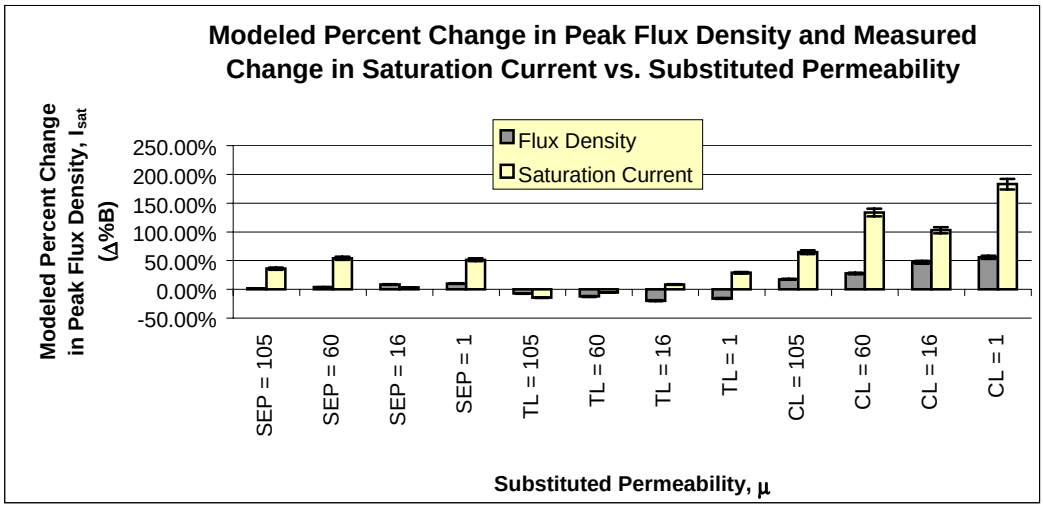

Figure [49] Comparison of modeled percent change in peak flux density to measured percent changes in saturation currents for various substitution methods.

This graph indicates that the initial assumption holds true only for substitutions made in the transmission line layer where there is a decreasing trend in flux density and an increasing trend n saturation current. For substitutions in the separating plane, and the cladding plane, the measured saturation current increases for increased peak flux density, which is counter to the original hypothesis. These two results are explained now.

Substitution of a low-permeability material into the separating layer has the effect of isolating one coil from the other, decoupling them. This decoupling produces a shorter magnetic path length, and results in higher flux densities. When a low permeability material is substituted into the cladding layers, a large volume fraction of the core material (~50%) is composed of the low permeability material. Such materials naturally saturate at higher magnetic fields, see Figure [5], and also give a correspondingly low inductance. The above measurements were compared to models constructed using linear material assumptions, and, in general, refuted the predictions of the model.

iv. Discrepancies

Neither of the models was completely accurate, however and discrepancies still exist. One of the most important reasons for these discrepancies is the inability to model inductors using both non-linear material properties and a time-varying signal at the same time. Another cause for discrepancy lies in the inability to measure saturation currents using a signal wherein both the current and frequency can be varied. If these issues could be addressed, then both the modeling and characterization of integrated thick film inductors could be improved.

c.) Volume fraction of substituted material

i. Analytical prediction

Self inductance, L, is proportional to the total magnetic flux which is related to permeability and magnetic field intensity through:

$$\Phi = \oint \mu_1 \bullet H_1 dA_1 + \oint \mu_2 \bullet H_2 dA_2 + ... \qquad \text{Eq.[18]}$$

Each term on the right represents a different material through which the magnetic flux flows. Increasing the volume fraction of low permeability materials will reduce the total flux and thereby increase the saturation current. The inductance value also decreases with an increased volume fraction of low permeability material.

ii. Discrepancies

Both finite element modeling and experimental measurements confirm, not surprisingly, that increasing the volume fraction of low permeability material increases the saturation current and lowers the inductance. We will now briefly discuss the mechanisms that cause this.

Low permeability material naturally has a higher saturation magnetization than high permeability materials. Figure [5] and Table[3] demonstrate this schematically.

Table [3] Values of saturation magnetizations for the materials under investigation.

Material	Saturation Magnetization (A/m)
IP9220	727
IP9105	1503
IP9060	1588
IP9016	3639

When large volume fractions (~50%) of low permeability materials are substituted into the structure, as in cladding layer substitutions, then a large portion of the measured self inductance is a result of the low permeability material. This has two significant effects. First, since the permeability

is lower, larger increases in current (magnetic field intensity) are required to produce changes in flux density. This effect tends to stabilize the measured inductance over a wide range of currents. Secondly, also owing to the reduced permeability, the nominal inductance is much lower, and closer to that of a non-magnetic core structure. Higher currents are therefore required to reach the 30% reduction from nominal inductance.

3.) Future experiments that might more accurately predict saturation current

To improve the accuracy of computer models that predict saturation current, non-linear material properties and a time-dependent current must be combined in the same model. It is possible to artificially simulate a high frequency current distribution in a DC current model, however, these models become very large and difficult to manage once solved. It may be possible to construct simpler models, with smaller solution matrices, from which the saturation current of a more complicated structure may be extrapolated.

C. Variations in inductance

1.) Introduction

Another key parameter under investigation was the total self-inductance. For maximum performance density, it is desired to combine a high volumetric inductance with a high saturation current. In the following section, the optimization of self-inductance will be discussed.
Self inductance, the parameter of interest for inductance measurements, is related to the total magnetic flux through Eq.[1] and Eq.[9]. From this relationship, we note that the inductance, L, can be increased by increasing the total flux produced by a given current. This flux can be expressed by the following equation:

$$\Phi = \frac{\mu \cdot H}{A} \qquad \text{Eq.[19]}$$

Here we see that two variables, permeability (μ) and cross sectional area (A), operate together to produce the total flux. As seen above, however, these two parameters are inversely related to each other such that as one acts to increase flux, the other decreases total flux. The net result is that there exists some optimal trade off between cross sectional area and permeability that produces a local maximum of inductance. Figure [50] and Figure [51], respectively, graphically represent how this maximum was both predicted by computer modeling, and verified by experimental measurements.

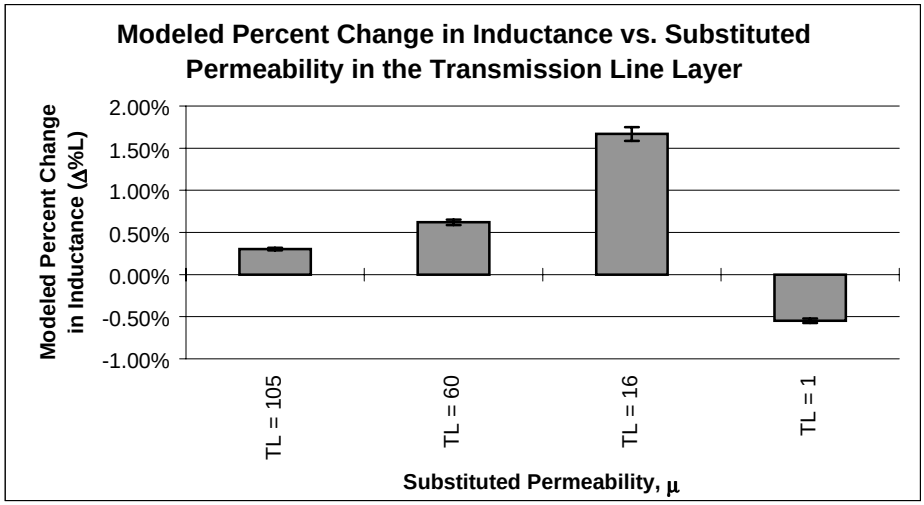

Figure [50] Modeled percent change in inductance for materials with decreasing permeabilities substituted into the TL plane.

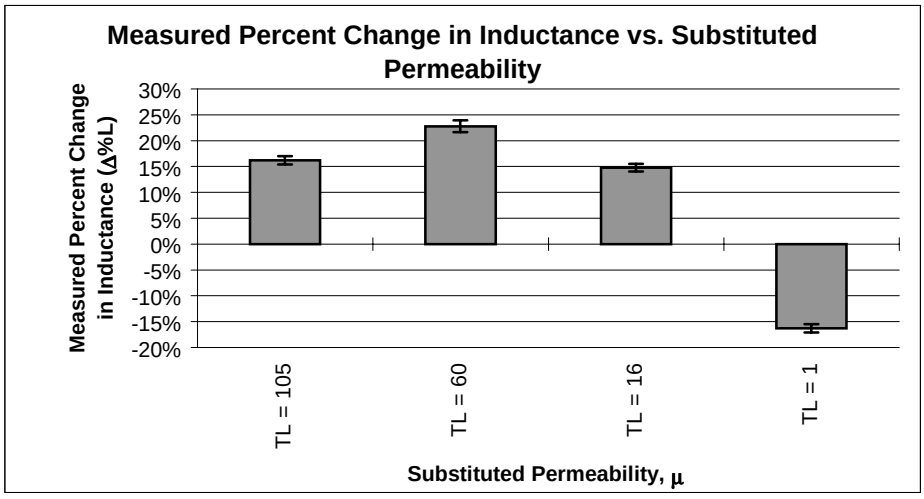

Figure [51] Measured percent change in inductance for materials with decreasing permeabilities substituted into the TL plane.

2.) Interpretations of experimental results using fundamental principles and computer models

a.) Magnetic path length

The first feature to be considered in the effects on self-inductance is the magnetic path length. Specifically, the contribution of an element of material located at some distance away from the conductor will be examined. To maximize the volumetric performance of these inductors, the flux inside the core will be optimized such that each element contributes a maximum possible value to the total self-inductance.

i. Analytical prediction

As stated above:

$$L = \frac{d\Phi}{dI} \qquad \text{Eq.[4]}$$

and

$$H = \frac{I}{l} \qquad \text{Eq.[8]}$$

Thus, for a given current in the conductor, the magnetic field intensity, H, in the vicinity of the conductor is fixed by the magnetic path length, which is, in turn, fixed by the distance from the conductor. It has also been shown that dΦ varies with permeability, which in a non-linear material varies with H. The result is that the self-inductance contributed by an element of material in the core will only be optimized if the value of μ in the element lies within its optimal region as determined by the magnetic field.

$$\Phi = \oint \mu_1 \bullet H_1 dA_1 + \oint \mu_2 \bullet H_2 dA_2 + ... \qquad \text{Eq.[18]}$$

The analytical solution, then, predicts that self-inductance may be increased if a low permeability material is used close to the conductor instead of a high permeability material.

ii. Finite element modeling

The finite element model that describes this best is one wherein the low permeability material is substituted into the transmission line plane. The magnetic path length around a current carrying conductor is related to the cross-sectional area of the magnetic path, and, therefore, as the area increases, so does the magnetic path length. Figure [46] shows the distribution of the magnetic field about a conductor where a low permeability material has been substituted into the conducting layer. Figure [50] contains a graph of the modeled inductance vs. the permeability substituted into the conducting layer. As can be seen, there is a maximum value for the percent change in inductance. This corresponds to the optimal trade off, for this structure, between a high permeability, and a long magnetic path length (large area) for the magnetic field. The computer model predicts that this maximum will occur when a permeability of $\mu = 16$ is substituted into the transmission line layer.

iii. Experimental verification

The experimental measurements confirmed the existence of a peak, however the substituted permeability at which the peak occurred was observed to be at $\mu = 60$, instead of $\mu = 16$. Figures [50], and [51] contain graphs comparing the modeled vs. measured changes in self-inductance for selected permeabilities of the transmission line layer.

iv. Discrepancies

The differences between the models, such as the magnitude of variation, and the permeability at which the peak exists, lay in the errors in modeling noted above. The important feature to note is that a peak exists, which indicates that there is a design feature that can be optimized to get the highest performance possible out of the structures being studied.

b.) Magnetic coupling

Another quantity that affects the inductance of a multi-coil inductor is the amount of coupling between the coils. The coupling describes the degree to which the magnetic field circulates around parallel, non-coaxial conductors. A coupling value of 1.0 indicates perfect coupling, while zero indicates no coupling. In a perfectly coupled pair of current-carrying conductors, no magnetic field circulates between the conductors, rather, all of the magnetic field circulates around the outside of both conductors. Figures [52], (a) and (b) respectively show the magnetic path of perfectly coupled planar conductors[11].

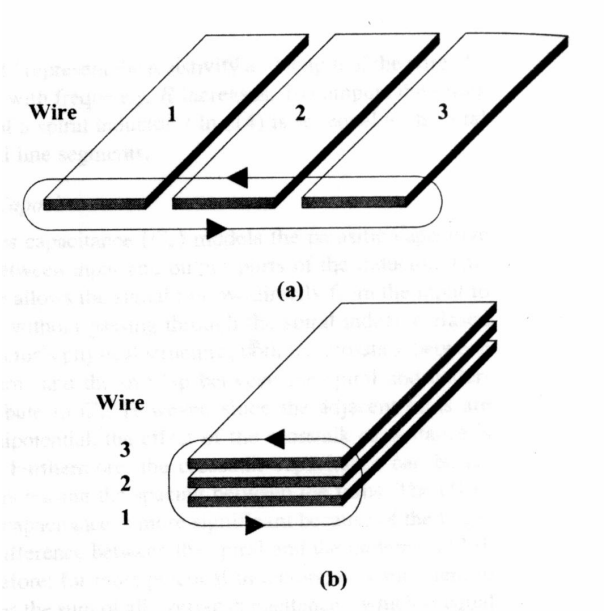

Figure [52] Magnetic path of a perfectly coupled coplanar (a) and parallel, non-coplanar (b) current-carrying conductors[11].

The standard equation for the inductance of a wire-wound solenoid is given by:

$$L = \frac{\mu N^2 A}{l} \qquad \text{Eq.[20]}$$

Where:

L = self inductance N = number of coupled turns

A = cross-sectional area L = length of solenoid

This equation assumes that all the conductors are perfectly coupled. For a wire-wound inductor, this is an acceptable approximation. For a printed inductor with planar conductive traces, the traces are not perfectly coupled and inductance decreases as a result. If the magnetic field inside the core can be redistributed such that coupling is improved, then inductance will improve as well.

i. Analytical Prediction

In a coiled inductor, formed by wrapping a current carrying conductor around a magnetic core, the self-inductance is proportional to the number of magnetically coupled turns as:

$$L = \frac{N\Phi}{I} \qquad \text{Eq.[21]}$$

Where:

L = self inductance N = number of magnetically coupled turns

If these coils are uncoupled, then they act independently. In the case where a low permeability material was substituted into the separating layer directly between the transmission line coils, the saturation current is observed to increase to approximately 40% greater than the baseline, but does not vary significantly as lower permeability materials were inserted. This stability was due to the de-coupling effect produced by the location of the low permeability material, after which the coils did not measurably interact. With no coil interaction, further reduction of substituted permeability resulted in no further change in saturation current.

ii. Finite element modeling

Referring back to Figure [46], it can be seen that as the permeability of the transmission line layer is reduced, the magnetic field redistributes between the conductors in the same plane. This indicates that more of the magnetic field is circulating around adjacent conductors instead of around individual conductors. Finite element models were used to calculate the coupling coefficient between

conductors of several models. However, due to the limitations of the modeling software, the coupling coefficient for conductors carrying a high-frequency signal could not be calculated.

iii. Experimental verification

One series of experimental samples that can verify the above model is one wherein the permeability of the transmission line layer is varied from $\mu = 105$ to $\mu = 16$. In these samples, we observe that as the permeability of the transmission line is reduced, the inductance increases. This increase is due, in part, to the increased coupling between the transmission lines. Figure [51] contains a summary of these results. When permeability is decreased to $\mu = 16$, the inductance again decreases due to mechanisms described above.

iv. Discrepancies

One of the difficulties in identifying exactly which mechanism is at work to force a change in the measured results, is that several mechanisms are operating simultaneously at all times. If the exact and isolated effect of material substitution on the coupling coefficient is to be quantified, then simple models and experimental devices must be created that hold other variables constant.

3.) Future experiments that might more clearly isolate mechanisms

In this research, it has become apparent that the modeling and characterization of integrated thick film inductors is a complex task, requiring the consideration of multiple factors and fundamental principles of electromagnetics. The scope of this research was limited such that it was not always possible to clearly identify the mechanisms responsible for variations in the experimental measurements. In the section following, several suggestions are presented to aid future researchers to more carefully proceed, and to enable them to make more definite conclusions.

a.) "Fundamental" geometries

One of the most critical obstacles to identifying and quantifying the effects of various mechanisms on inductance is their interaction. In the complex geometry of a real thick film planar inductor, several mechanisms are operating simultaneously and cannot be separated. The same difficulty applies in analytical and finite element modeling. To address this challenge, computer models and test devices must be created using "fundamental" geometries wherein the interaction of multiple mechanisms can be eliminated.

b.) Different placement of material

One of the more interesting implications of the analytical predictions is that the electromagnetic performance of a device will vary with the magnetic properties of the material surrounding the conductors largely as a function of the material's distance from the conductor. In the present research, material placement has been limited to discrete layers. To more accurately validate the analytical predictions, it would be beneficial to deposit material symmetrically about a cylindrical current carrying conductor (i.e. a wire). The material properties of the magnetic properties should be varied as a function of the radial distance from the center of the conductor. Such a structure would allow direct verification of the analytical solutions, and would also be extremely simple to model using finite element analysis.

c.) Variable current and frequency test signal

The characterization of the inductors produced in this research was limited due to the inability to combine a variable frequency and variable current test signal. Such measurements are not trivial, but are required to fully validate computer models. It may be possible to construct test equipment based on a calculated response of a system, which includes the test inductor, if all the other components of the system are accurately characterized.

d.) More advanced finite element modeling tools

The finite element computer modeling could be improved to combine non-linear material properties with the current distribution produced by a high frequency test signal. In this research, a series of models was constructed to accomplish such a combination. The composite models produced, however, proved too cumbersome to manage. Reducing the number of conductors in the model and increasing the number of elements per conductor could be used in future working composite models.

V. Chapter 5: Conclusions

There arose three primary observations from this research, they are: 1) finite element analysis, supplemented with analytical calculations based on first principles, can be used effectively to predict the performance of inductors with magnetic composite core structures, 2) magnetic composite cores have been demonstrated, experimentally, to yield improvements in saturation current and / or inductance, and 3) the operation of several different mechanisms is responsible for the performance of magnetic devices with inhomogeneous cores.

A. Success of computer modeling

The use of finite element method computer modeling predicted magnetic flux distributions that could be used, with the aid of fundamental principles, to predict the performance of magnetic composite core inductors. This is a significant realization in that without predictive modeling, it would be much more difficult to make effective design modifications to this type of structure.

B. Success of experimental results

The experimental results confirm the modeled predictions that improvements can be made in saturation current, inductance, or both. Most structures resulted in a balance between these two measurements, meaning that improvements in saturation current usually resulted in a loss of inductance. There was one structure, however, that produced increases in both inductance and saturation current. Furthermore, the balance was not always equal. In one structure, an increase in saturation current of 133% was observed with only a 12% decrease in inductance.

C. Operating mechanisms identified

Using fundamental principles to correlate modeled predictions with measured results, it was observed that the operation of several different mechanisms was responsible for the performance of magnetic devices with inhomogeneous cores. Simple assumptions based on the earlier models were

inadequate to predict the measured performance of the test inductors. However, on closer examination, and after including secondary effects not initially considered, at least three different operating mechanisms were identified including: 1) peak flux density in a given region of magnetic material, 2) volume fraction of the substituted material, and 3) the effect of de-coupling current carrying conductors.

VI. Chapter 6: Summary

The objective of this project was to develop magnetic devices for electronic systems that have a higher volumetric performance and that integrate easily with state of the art hybrid circuit packages. This objective was addressed in four broad phases. First, analytical predictions were made based on fundamental principles of electromagnetics to show that the performance of small inductors may be improved by using more than one different type of magnetic material to construct the core. Second, computer modeling was performed to optimize device structure. Third, test devices were produced using thick film processing. Finally, devices were tested to evaluate their performance and the validity of the computer models.

Using finite element modeling, the effect on performance related to geometry, material characteristics, and operating frequency was examined. Specifically, the effects of using multiple permeability materials were considered. With modeling completed, several designs were selected for production. Finished devices were tested for electromagnetic performance.

Variations in saturation current and inductance were measured for each series of substitutional strategy. The results from both the modeled structures, and the measured test inductors may be summarized as follows: Varying the permeability in selected regions resulted in increases in saturation current, inductance, or both. In all but one case, increasing saturation current resulted in decreasing inductance, and vice versa. Comparisons were made against a base line model, which consisted of a single material core, with a permeability of 220.

Measured changes in saturation current and inductance were analyzed. It was shown that in some cases the initial assumptions were too simple to predict actual performance, but that fundamental principles of electromagnetics can be used to more carefully analyze the modeled data and to explain the measured results. More complete assumptions and explanations were presented to describe the correlation between the computer models and the experimental results.

There arose three primary observations from this research, they are: 1) finite element analysis can be used effectively to predict the performance of inductors with magnetic composite core structures, 2) magnetic composite cores have been demonstrated, experimentally, to yield improvements in saturation current and / or inductance, and 3) the operation of several different mechanisms is responsible for the performance of magnetic devices with inhomogeneous cores.

VII. References

1.) Harrer, J, and Ray Petit, "RF Characterization of Thick Film for Portable Transceivers, The IMAPS Journal of Microcircuits and Electronic Packaging," Vol. 20, No. 2, 2nd quarter 1997.

2.) Webb, Denis C, "Status of Ferrite Technology for High Volume Microwave Applications, Materials and Processes for Wireless Communications," Ceramic Transactions, Vol. 53.

3.) Raffaelli, L., "Millimeter Wave Radio Front Ends: The Present and the Future," Microwave Journal, Vol. 42, No. 6, June 1999.

4.) Park, Jae Y, and Mark g. Allen, "Packaging Compatible Micromagnetic Devices Using Screen Printed Polymer/Ferrite," The International Journal of Microcircuits and Electronic Packaging, Vol 21, No. 3, 3rd Quarter 1998.

5.) Heinrich, W. and H. Zscheile, "MMIC Spiral Inductor Modeling," Microwave Journal, May 1996.

6.) AVX Inc. "RF Microwave / Thin Film Products," Product information, AVX Inc, 2000.

7.) Neelakanta, Perambur S., "Handbook of Electromagnetic Materials: Monolithic and Composite Versions and Their Applications," CRC Press, New York, 1995.

8.) Yao, Kaiwei, Pit-leong Wong, and F.C. Lee, "Inductor Design for Multi-Channel Voltage Regulator Module," Center for Power Electronic Systems, 1999.

9.) Forman, Peter and Robert W. Saint John, "Creating Convergence," Scientific American, Vol. 283, November, 2000.

10.) Tarvainen, E., et. al., " 1.8 GHz Current-controlled Oscillator IC Implementated by Using Integrated Inductors and 0.8 μm BiCMOS Technology," IEE Electronics Letters, Vol. 32, No. 16, August 1996.

11.) Yue, Patrick C., and S. Simon Wong, "Physical Modeling of Spiral Inductors on Silicon," IEEE Transactions on Electron Devices, Vol. 47, No. 3, March 2000.

12.) Lovelace, David, Natalino Camilleri, and George Kannell, "Silicon MMIC Inductor Modeling for High Volume, Low Cost Applications," Microwave Journal, August 1994.

13.) Kuhn, William B. and Naveen K. Yanduru, "Spiral Inductor Substrate Loss Modeling in Silicon RFICs," Microwave Journal, March 1999.

14.) Odendaal, W. G. "A Generic Approach for the Modelling of High Power Density Magnetic Components," Thesis, Department of Electrical and Electronic Engineering, Rand Afrikaans University, Johannesburg, South Africa, 1997.

15.) Tsutaoka, Takanori, Tatsuya Nakamura, and Kenichi Hatakeyama, "Frequency Dispersion and Temperature Variation of Complex Permeability of Ni-Zn Ferrite Composite Materials," Journal of Applied Physics, Vol. 78, No. 6, September 15, 1995.

16.) Rado, G. T. Rev. Modern Physics, Vol 25, No. 81, 1953.

17.) Bouchaud, J. P. and P. G. Zerah, Journal of Applied Physics, Vol 67, 1990

18.) Morgenthaler, Frederic R., "An Overview of Electromagnetic and Spin Angular Momentum Mechanical Waves in Ferrite Media," Proceedings of the IEEE, Vol. 76, No. 2, February, 1988.

19.) Gaiewski, W. R., L.P. Dunleavy, and L. A. Geis, "Hybrid Inductor Modeling for Successful Filter Design," IEEE Transactions on Microwave Theory and Techniques, Vol. 42, No. 7, July 1994.

20.) Harada, Mitsuru, Hikara Yamaguchi, and Toshiaki Tsuchiya, “Investigation of a Multigigahertz MOSFET Amplifier with an On-chip Inductor Fabricated on a SIMOX Wafer,” IEEE Transactions on Electron Devices, Vol. 45, No. 1, January 1998.

21.) Rittweger, M. and I. Wolff, “Analysis of Complex Passive MMIC Components Using the Finite-difference Time-domain Approach,” IEEE International Microwave Symposium Digest, 1990, Vol. III.

22.) Schmuckle, F.J., and R. Pregla, “The Method of Lines for the Rigorous Full Wave Analysis of Rectangular Bends of Mjultiple-line Systems,” IEEE International Microwave Symposium Digest, 1992, Vol. II.

23.) Kashani, Mohammad Mansour Riahi, “Formulation, Development, and Characterization of Magnetic Pastes and Epoxies for Thick Film Inductors,” Dissertation, Virginia Polytechnic Institute and State University, May 1992.

24.) Heraeus Cermalloy, Inc., “Ferrite Materials Information Data Book,” Heraeus Cermalloy, Inc.

25.) Lopez-Villegas, Jose M., “Improvement of the Quality Factor of RF Integrated Inductors by Layout Optimization,” IEEE Transactions on Microwave Theory and Techniques, Vol. 48, No. 1, January 2000.

26.) Reitz, John R., Frederick J. Milford, and Robert W. Christy, “Foundations of Electromagnetic Theory, Fourth Eddition,” Addison-Wesley Publishing Company, New York, 1992.

27.) Mr. Glenn Skutt, Magnetics Engineer, Virginia Power Technology Inc, Personal interview.

Vita

Robert Fielder will graduate with a Masters of Science degree in Materials Science and Engineering on December 15, 2000 from Virginia Polytechnic Institute and State University. Robert has specialized in electronic and magnetic materials and has worked as a research assistant in electronic packaging for most of his undergraduate and graduate career. Formerly a U.S. Navy nuclear mechanical operator, Robert is married and has two children.